

INFLUENCE OF DIAGENESIS ON THE QUALITY OF LOWER CRETACEOUS PRE-SALT LACUSTRINE CARBONATE RESERVOIRS FROM NORTHERN CAMPOS BASIN, OFFSHORE BRAZIL

RONALDO HERLINGER, JR.,¹ EVELINE ELLEN ZAMBONATO,² AND LUIZ FERNANDO DE ROS³

¹Petrobras S.A., Avenida República do Chile, 330, Rio de Janeiro, RJ, Brazil

²Petrobras S.A., Avenida Nossa Senhora da Penha, 1688, Barro Vermelho, Vitória, ES, Brazil

³Instituto de Geociências, Universidade Federal do Rio Grande do Sul, Porto Alegre, RS, Brazil

e-mail: ronaldo.herlinger@petrobras.com.br

ABSTRACT: The genesis and evolution of lacustrine pre-salt carbonate reservoirs, which contain giant hydrocarbon accumulations along the South Atlantic margins, has attracted major research interest. The huge extension and volume, and unusual textural and compositional features, are key elements for understanding the tectonic, structural, stratigraphic, and sedimentological generation and early evolution of the region, as well as potentially of other lacustrine carbonate systems. A systematic petrographic and petrophysical study has been performed on the Lower Cretaceous lacustrine carbonate reservoirs from northern Campos Basin, Offshore Brazil, in order to unravel the main controls on the origin and evolution of pore systems. The main lithologic types recognized in the rift section are bivalve–gastropod grainstones and rudstones, arenites constituted by ooids of syngenetic magnesian clay minerals (mostly stevensite), and dolostones, while stevensitic claystones with calcite spherulites, fascicular calcite crusts, intraclastic rudstones and grainstones, and dolostones are the main lithologic types in the sag section. The eogenetic evolution of bioclastic reservoirs was controlled by the balance between dissolution and neomorphism of the aragonitic bivalve and gastropod bioclasts, favoring either the generation of poorly connected moldic porosity or the preservation of well-connected interparticle porosity. The stevensitic arenites were strongly affected by meteoric dissolution and replacement by dolomite and silica, related to regional uplift and erosion after the rift phase, which generated highly heterogeneous pore systems with moldic, intercrystalline, vugular, and microcrystalline pores. Stevensitic claystones that are replaced by calcite spherulites and dolomite normally show low porosity, but locally constitute reservoirs, where secondary porosity was generated by stevensite dissolution. The precipitation of crystal shrubs of fascicular-optic calcite in coalescent crusts generated growth-framework primary porosity, which was reduced mostly by dolomite cementation, or enlarged by dissolution, enhancing their permeability. Non-coalescent calcite crusts contain abundant syngenetic magnesian clay minerals. Their porosity is related to dissolution of these clays, which generated poor permeability. Intraclastic grainstones and rudstones are compacted and cemented, or rich in clay matrix (“hybrid packstones”). Where they display preserved interparticle primary porosity or matrix dissolution, they may have good porosity and permeability. The heterogeneous dolomitization of both the rift and the sag deposits either destroyed their primary or early diagenetic porosity, or generated high porosity and permeability values in the dolostones. Relationships between replacement and compaction indicate that most of the diagenetic processes occurred during eodiagenesis, controlled mostly by the instability of the aragonite in the bioclastic reservoirs and of the stevensite in the claystones, ooidal arenites, and fascicular calcite crusts. This study characterizes the major primary and diagenetic aspects of the pre-salt reservoirs, providing insights on the evolution of their porosity and permeability. This is expected to contribute to the prediction of quality during exploration and to enhance hydrocarbon recovery from producing oilfields, as well as to increase the understanding of the origin, evolution, and quality distribution in analogous lacustrine reservoirs.

INTRODUCTION

In the last decade, giant hydrocarbon accumulations were discovered in lacustrine carbonate reservoirs below Aptian evaporites along the South Atlantic conjugate margins (Carminatti et al. 2009; Sallet et al. 2016). These reservoirs, together with important discoveries in China, have attracted significant interest in the exploration and scientific research of continental carbonates. The genesis and evolution of pre-salt reservoirs

represent a geologic enigma that has puzzled many major researchers, by their huge extension and volume, their unusual textural and compositional features, and by what they will reveal about the South Atlantic tectonic, structural, stratigraphic, and sedimentological generation and early evolution.

On the other hand, knowledge of continental carbonates is relatively restricted when compared to that of marine carbonates, which are much more voluminous and host giant reserves of hydrocarbons around the

world. In this sense, the recent discoveries of huge hydrocarbon accumulations in lacustrine carbonates from Brazil, Africa, and China have attracted intense scientific interest for a better understanding of the formation and evolutionary processes of these reservoirs.

Modern and ancient lacustrine carbonates are characterized by a great variability of facies and mineral species, having been studied for decades. Lacustrine carbonates strongly contrast with marine carbonates. While the main control on the environmental genetic conditions of marine carbonates is geological age (Moore 2001), lacustrine carbonates have their genesis controlled by local geological settings, such as tectonics, climate, fauna, and specific geochemical conditions that can form very particular deposits (Davis and Wilkinson 1983; De Wett et al. 2002; Dunagan and Turner 2004; Gierlowski-Kordesch 2009; Fedorchuk 2014). The deposition of lacustrine carbonates is controlled by several factors, including hydrological (input and output of surface waters, precipitation, and groundwater flow), sedimentary input, and temperature variations (Platt and Wright 1991; Tucker and Wright 1991). Water geochemistry plays a major role in lacustrine environments, because it controls a number of processes, including development of microbial communities (Riding and Liang 2005; Vasconcelos et al. 2006; Spadafora et al. 2010), abiotic precipitation of carbonates (Riding 2008; Wright and Barnett 2015) and clay minerals (Calvo et al. 1999; Pozo and Casas 1999; Furquim et al. 2008), and the development of algae, ostracodes, and mollusks (bivalves or gastropods) (Casanova 1986; Renaut et al. 1986; Vincens et al. 1986; Harris et al. 1994; Frogley et al. 2002).

The pore systems of carbonate reservoirs, both continental and marine, show great diversity of pore types, and wide heterogeneity (Choquette and Pray 1970; Mazzullo and Harris 1991; Lucia 1995; Moore 2001; Mazzullo 2004; Lønøy 2006; Ahr 2008). Porosity is controlled by many factors, including the interplay of physical, chemical, and biological depositional processes, which are overprinted by intense diagenesis due to the chemical reactivity of carbonates, as well as by fracturing and hydrothermal processes (Ehrenberg et al. 2006; Ehrenberg et al. 2012; Chafetz 2013; Bragaud et al. 2014). In most cases, the porosity evolution patterns are controlled by a combination of mineral composition, fabric, and diagenetic conditions. The carbonate permeability frequently correlates poorly with porosity, due to heterogeneous porous framework, where the original fabric can be intensely modified by diagenetic processes (Dürrast and Siegesmund 1999; Weger et al. 2009; van der Land et al. 2013; Rezende and Pope 2015). The study of porosity geometry is important in characterization of carbonate reservoirs, supporting petrophysical interpretation and improving predictability of reservoir quality and heterogeneity (Basan et al. 1997; Mountjoy and Marquez 1997; Eichenseer et al. 1999; Machel 2005).

The aim of this work is to discuss the impact of diagenesis on the evolution of porosity and permeability of pre-salt lacustrine carbonates from northern Campos Basin, through the combination of petrographic and petrophysical analyses. This work contributes to the prediction of quality during exploration and aims to enhance recovery from producing oilfields, as well as to increase the understanding of the origin, evolution, and quality distribution in analogous lacustrine reservoirs worldwide.

GEOLOGICAL SETTING

The Campos Basin is a passive-margin basin situated on the northern coast of the Rio de Janeiro State, Brazil (Fig. 1A), extending to the southern coast of the Espírito Santo State, being geographically located between parallels 21° and 23° S. The basin is located between the Santos Basin to the south, bounded by the Cabo Frio volcanic high, and the Espírito Santo Basin to the north, bounded by the Vitória High.

The Campos Basin was formed under an extensional tectonic regime during the breakup of the Gondwana Continent during Late Jurassic–Early Cretaceous, preceding the final separation of South America and Africa,

and the formation of the South Atlantic Ocean (Rabinowitz and LaBrecque 1979; Austin and Uchupi 1982; Nürnberg and Müller 1991; Cainelli and Mohriak 1999; Guardado et al. 2000). The formation of the Atlantic Ocean started with crustal thinning and breakup of São Francisco–Congo–Rio de La Plata–Kalahari cratons, accreted during the Eoproterozoic orogeny. South Atlantic formation began during the Jurassic with rifting between Argentina and southern Africa, and through the Equatorial Margin (Szatmari 2000; Meisling et al. 2001; Mohriak et al. 2008). The rupture of the central portion, controlled by a resistant cratonic core (São Francisco–Congo Craton), occurred later, in the Hauterivian (Clemson et al. 1997; Karner and Driscoll 1999), resulting in the development of a narrow rift zone in this region. The Santos, Espírito Santo, and Campos basins, located on a Proterozoic fold belt, developed wider basins (Mohriak et al. 2008; Rosendahl et al. 2005).

The Barremian to Aptian rift stage was characterized by increased lithospheric extension and asthenospheric uplift (McKenzie 1978; White and McKenzie 1988), associated with extensive intracratonic tholeiitic volcanism (Turner et al. 1994; Mohriak et al. 2008; Torsvik et al. 2009). Elongated deep lakes formed parallel to basement lineaments, and were filled with both volcanic and sedimentary rocks (Dias et al. 1988; Mizusaki et al. 1988). The presence of transfer zones played an important role in the partitioning of the rifted margin in subbasins (Meisling et al. 2001; Muniz 2014). The Aptian sag stage is preceded by uplift and erosion of the rift section, resulting in a regional unconformity (Karner and Driscoll 1999; Dias 2005; Winter et al. 2007). The initial sag sedimentation included carbonate, Mg-clays, and clastics, which are overlain by evaporites formed in an arid climate under influx of incursions of marine seawater (Abrahão and Warne 1990; Karner and Gambôa 2007). The last stage (drift phase) is characterized by the development of oceanic crust and a passive margin (Chang et al. 1988; Chang et al. 1992; Aslanian et al. 2009).

The Lagoa Feia Group, originally defined by Schaller (1973) as the Lagoa Feia Formation, unconformably overlies pre-rift flood basalts from the Cabiúnas Formation, comprising the nonmarine to transitional sequences from the Campos Basin. Subsequently, the Lagoa Feia Formation has been subdivided into four distinct depositional sequences bounded by unconformities, including: the Basal Clastic Sequence, the Talc-Stevensitic Sequence, the Coquinas Sequence, and the Clastic–Evaporitic Sequence (Dias et al. 1988). The last two sequences are separated by the pre-Alagoas unconformity. More recently, Winter et al. (2007) subdivided the Lagoa Feia Formation into several formations, elevating it to group status (Fig. 1B).

The rift phase Coqueiros Formation is composed mainly of bioclastic rudstones and grainstones, informally known as “coquinas,” interfingered with proximal clastic sediments of the Itabapoana Formation towards the western margin of the basin. The Coqueiros Formation consists mainly of bioclasts of bivalve mollusks, with subordinate amounts of gastropods and ostracods. Some authors have proposed depositional and sedimentological models of bioclastic deposits. Castro et al. (1981) separated the bioclastic deposits into two types: “detrital coquinas” consisting of bioclasts and noncarbonate grains (talc-stevensite ooids and peloids and mud intraclasts); and “pure coquinas,” composed entirely of bioclasts. Bertani and Carozzi (1985a) recognized several microfacies, separating sequences dominated by bivalves and by ostracods, and according to variations on composition, grain size, matrix, and cement content. These authors related the distribution of microfacies to two distinct depositional models: playa-lake settings dominated by ostracods, and pluvial-lake settings dominated by bivalve mollusks. Carvalho et al. (2000) recognized seven main depositional environments based on facies associations, including bioclastic beaches, bioclastic sandy beaches and marginal lacustrine settings, bioclastic sheet and bar fringes, consisting of shell debris deposited by storm events, bioaccumulation banks, and deep lacustrine settings. Recently, Goldberg et al. (2017) interpreted, based on the integration of quantitative petrography, sedimentology, and seismic

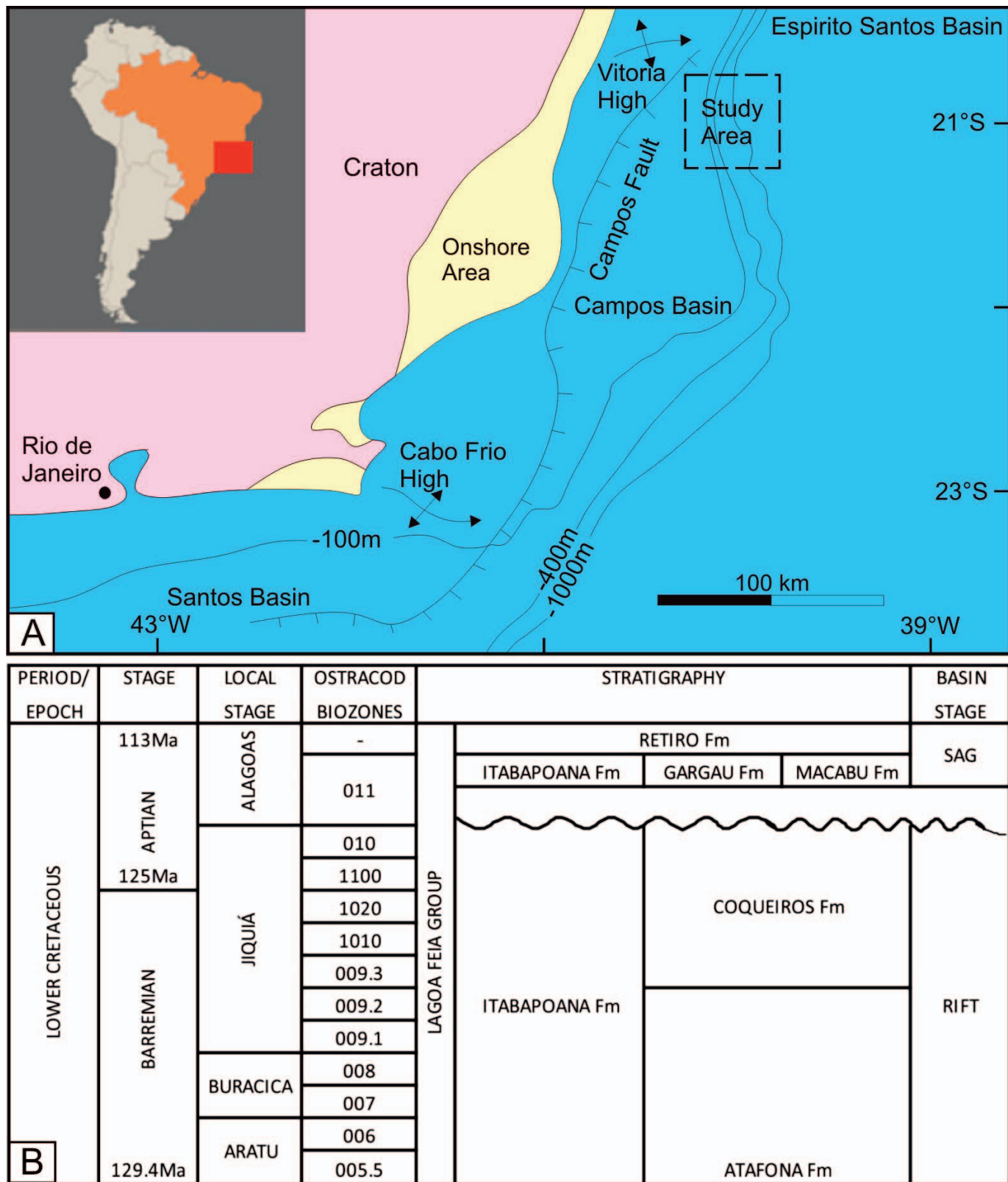


FIG. 1.—A) Location of the Campos Basin and the study area (modified from Dias et al. 1988). B) Biozones (Moura and Praça 1985; Silva-Telles 1992) and stratigraphy of the Lagoa Feia Group (Winter et al. 2007).

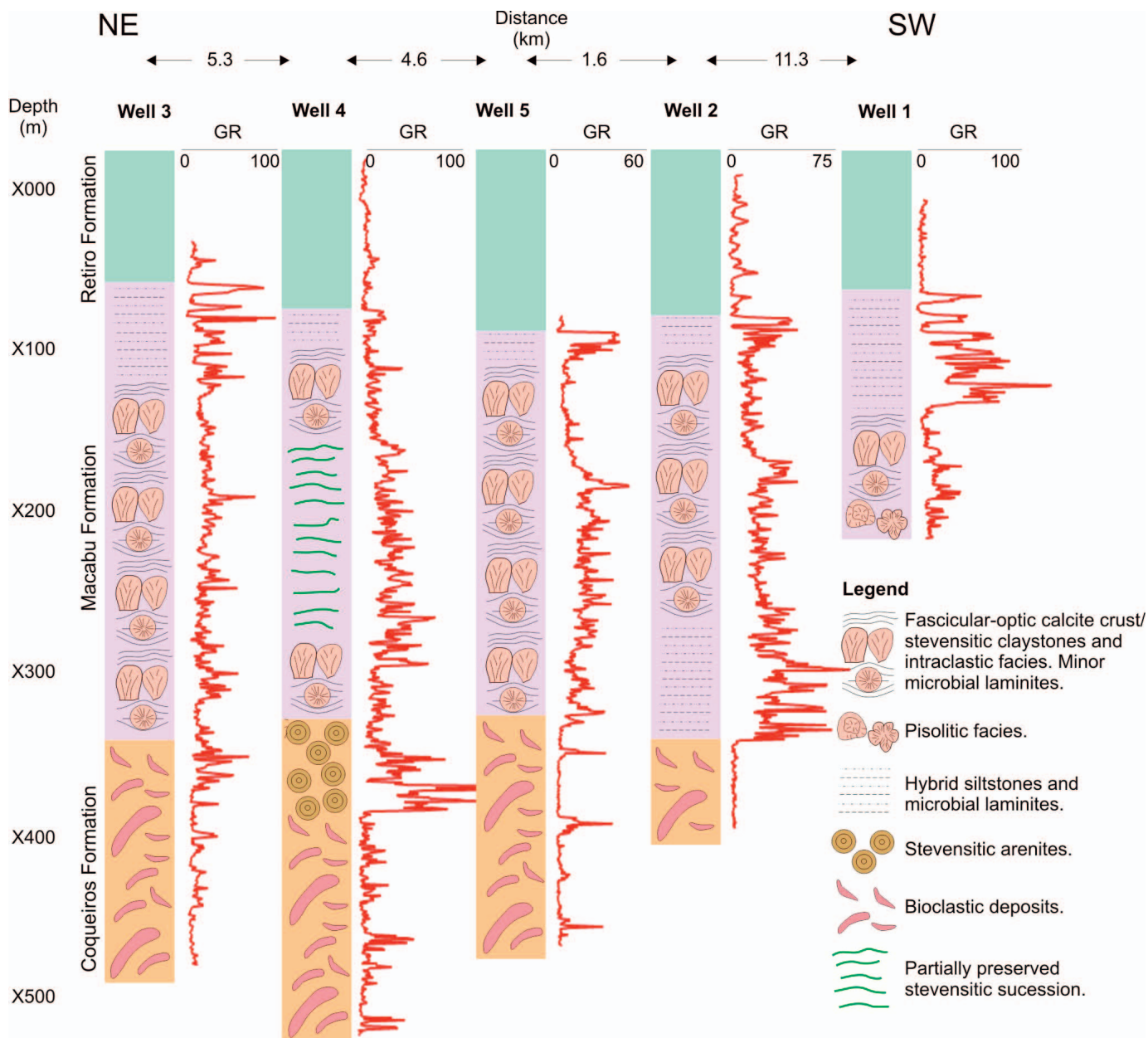


FIG. 2.—Schematic correlation of the studied wells, showing distance between wells, units, gamma ray logs, and facies succession.

stratigraphy, that the bioclastic rudstones correspond mostly to gravitational deposits, resedimented from structural highs to deeper lacustrine settings, throughout the rift section of the basin.

Sag phase deposits from the Macabu Formation were referred to by Dias et al. (1988) as carbonate facies consisting of nodular diagenetic limestones and laminated limestones, “probably algal in origin (stromatolites).” Later, Dias (2005) interpreted laminites and microbial stromatolites as supratidal and upper-intertidal facies, overlain by lower-intertidal clay-rich facies and subtidal mudstones deposited in an epicontinental context with extensive pre-evaporitic clastics located in shallow proximal regions. Muniz and Bosence (2015) interpreted the absence of both marine biota and normal freshwater biota, such as charophytes, and the presence of nonmarine ostracods, as evidence of a brackish-water–lacustrine environment, refuting the presence of tidal influence on microbial development. However, recent interpretation suggests that most deposits from the

Macabu Formation are chemical precipitates, controlled by the geochemistry of alkaline lacustrine waters (Wright 2011, 2012, 2013; Tosca and Wright 2014). Wright and Barnett (2015) identified a typical cyclothem as composed of three main components: mud-grade laminated carbonates, accumulated in flooding phase, calcite spherulites in a matrix of Mg-silicates, and calcitic shrub-like growths triggered by evaporation, controlled by pH and ionic activity.

METHODS

This study is based on 780 samples from cores and sidewall plugs collected from five wells (Fig. 2). The applied methods include optical petrography (plane-polarized light (PL); crossed-polarized light (XPL)), ultraviolet fluorescence (UVF), cathodoluminescence (CL), scanning electron microscopy (SEM), X-ray diffraction (XRD), and petrophysical

analysis. In order to characterize the primary and diagenetic constituents, the pore types, and their relationships, optical petrography was performed on thin sections impregnated with blue epoxy resin. 139 thin sections were quantified and described in detail, and 641 thin sections were classified according main constituents, textures, and pore types. Pore types were classified according to Choquette and Pray (1970). Thin sections were stained for carbonate identification with an acid solution of alizarin red and potassium ferrocyanide (Dickson 1965). A Zeiss Colibri fluorescence light-emitting-diode (LED) UV microscope was used to evaluate presence of organic matter and relations of replacement between fluorescent minerals. In order to identify diagenetic carbonate phases, cathodoluminescence (CL) microscopy was performed in a Cambridge Image Technology Ltd. (CITL) luminoscope. CL analyses were performed in CL8200 MK5-2 equipment coupled to Leica microscope, under operating conditions of 300 mA and 17 kV. Scanning electron microscopy (SEM) analyses using backscattered and secondary electrons were executed in ZEISS EVO LS15 or JEOL JSM 6490LV electron microscopes, both equipped with OXFORD Inca/Aztec energy-dispersed spectrometers (EDS), in order to investigate paragenetic relationships between primary and diagenetic constituents, and to identify the elemental mineral composition in representative rock fragments and thin sections. X-ray diffraction (XRD) analyses of the clay fraction, including air-dried, glycol-saturated, and heated treatments, were used to confirm the clay-mineral species. Petrophysical analyses were performed on plugs cut from cores and on sidewall cores in order to determine porosity and permeability according to norm API RP 40:1998. Mercury injection capillary pressure (MICP) analyses were performed on a Micrometrics AutoPore IV 9500 equipment to determine the pore-throat size distribution of representative samples.

RESULTS

Petrography

The studied reservoirs in the rift section are composed of massive bioclastic rudstones and grainstones (“coquinas”), about 80 meters thick, and by stvensitic arenites that occur at the top of the section, described only in Well 4 (Fig. 2). Overlying these reservoirs, there are crusts of calcite shrubs and stvensitic claystones that occur in millimetric to decimetric intercalations. Additionally, intraclastic grainstones and rudstones of reworked spherulites and fragments of the crusts are found intercalated with the calcite crusts and stvensitic claystones. Hybrid siltstones, siliciclastic siltstones and claystones, and microbial laminites are concentrated at the top of the sag section and at the bottom of Well 2, and are not considered reservoirs.

Bivalve–Gastropod Rudstones and Grainstones (“Coquinas”).—The bioclastic grainstones (9% of the samples) and rudstones (91% of the samples) are mostly massive, poorly to well sorted, with a chaotic or subparallel fabric. The primary constituents are bioclasts of bivalves, gastropods, and ostracods. Bivalves are the main component, composing 100% of primary constituents in 64% of the samples (Fig. 3A). Bivalves always occur disarticulated, and their degree of reworking is widely variable. Bivalve bioclasts are frequently broken or dissolved, and have dimensions ranging from 0.07 to 25 mm (average = 2.3 mm) in the thin sections.

Gastropods are observed in 36% of the samples and are typically whole and not abraded (Fig. 3B), with preserved intraparticle porosity. The ostracod bioclasts are whole, sometimes articulated, and occasionally recrystallized. Ostracods occur in 8% of the samples and are the main primary component of grainstones (Fig. 3C) in two samples. Intraclasts of carbonate mud, volcanic, and siliciclastic grains occur in small amounts in the bioclastic rudstones and grainstones.

Calcite is the main cement of bioclastic rudstones and grainstones. The bioclasts are covered by continuous rims of microcrystalline to prismatic calcite (Fig. 3D). Drusy calcite frequently is the main interparticle cement. Dissolution of bioclasts generates intraparticle and moldic pores, which are filled by drusy (Fig. 3E) and blocky calcite. Subordinate cements that have filled interparticle pores include blocky, coarse mosaic, and microcrystalline calcite. Recrystallization of the bivalve and gastropod bioclasts to blocky calcite is common, masking the original fabric of the bioclastic rudstones and grainstones. Bivalves are dull CL, whilst intraparticle and interparticle cements are red in CL (Fig. 3F).

Bivalves and gastropods were either dissolved or neomorphosed (calcitized), commonly showing a heterogeneous range from total dissolution, with variable intensity of calcite cementation of the intra-particle and moldic porosity, to total neomorphism. The distinction between neomorphism and moldic pores cementation is, in many cases, difficult without CL. Calcitization of aragonitic bivalve and gastropod bioclasts often forms a mosaic of calcite crystals marked by fine lines of inclusions delineating the original structure of the shell (Fig. 3D). In contrast, the intraparticle and moldic pores were filled by drusiform (Fig. 3E) and blocky calcite. Dolomite occurs in 15% of the samples as a minor constituent (< 5%) in the bioclastic rudstones and grainstones of Wells 3 and 5 and more rarely in Well 2. Blocky and saddle dolomite fill locally interparticle, intraparticle, moldic, and vugular pores. Dolostones up to 10 meters thick occur in Well 5 as a product of replacement of the bioclastic rocks. These rocks are composed of small rhombohedral and, rarely, of saddle dolomite crystals. Sucrosic dolostones preserve partially the shape of the bioclasts (Fig. 4A).

Silica occurs in 44% of the samples, rarely making up more than 2% of the rock volume. Chalcedony and quartz (as blocky, prismatic, coarse mosaic, and microcrystalline), often occur in small amounts, mainly replacing calcite and rarely filling interparticle, intraparticle, moldic, and vugular porosity in bioclastic rudstones and grainstones. Microcrystalline quartz rims locally cover bioclasts. Drusy quartz locally fills moldic and vugular porosity. Displacive pore-filling interparticle quartz cement was observed in 4% of the samples (Fig. 4B).

Bioclastic grainstones and rudstones have a poor diversity of diagenetic minerals. Barite (BaSO_4) and celestine (SrSO_4) are rare, filling interparticle porosity or replacing calcite cements and bivalves. The aluminum-phosphate-sulfate (APS) minerals svanbergite ($\text{SrAl}_3(\text{PO}_4/\text{SO}_4)_2(\text{OH})_6$) and goyazite ($\text{SrHAl}_3(\text{PO}_4)_2(\text{OH})_6$) locally replace mud intraclasts (Fig. 4C) in bioclastic rudstones.

The main pore types in bioclastic rudstones are interparticle, intra-particle, moldic, and vugular (Figs. 3A, D, E, 4D, E). Bioclastic grainstones have predominantly intercrystalline and moldic porosity (Figs. 3C, 4F). Dolomitized rudstones and grainstones are both rich in intercrystalline porosity (Fig. 4A). Well 2 shows a cyclical variation of predominant pore types along the studied interval, from moldic to interparticle and to moldic again. The samples of Well 3 display predominance of moldic porosity, and those of Well 5, of interparticle porosity. Well 1 was not sampled in the bioclastic succession, and Well 4 was poorly sampled.

Stvensitic Arenites.—Massive, well to moderately sorted arenites composed of stvensitic ooids and stvensite-coated carbonate particles occur at the top of the rift section, only in Well 4, forming an interval about 50 meters thick (Fig. 2). The occurrence of these ooids is very common in the rift section of the Campos Basin. Previous studies pointed to a composition of stvensite, kerolite, and talc for such ooids (Bertani and Carozzi 1985a, 1985b; Rehim et al. 1986; Abrahão and Warne 1990; Armeleenti et al. 2016). These clay ooids are commonly dissolved and replaced by dolomite and quartz, and often are deformed. The diagenetic patterns of the stvensitic arenites are very heterogeneous. Frequently the ooids are cemented by dolomite or quartz, and almost completely silicified,

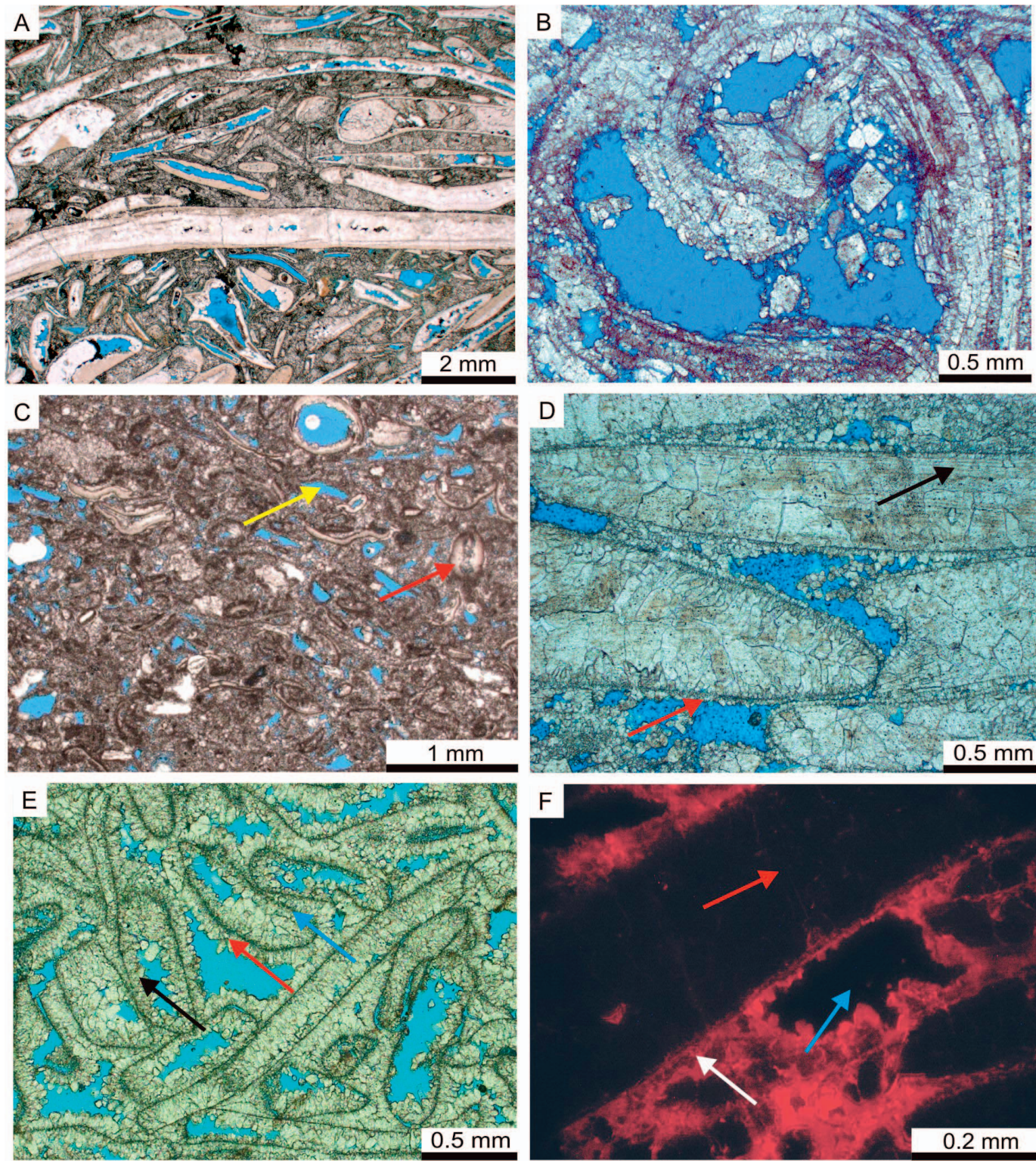


FIG. 3.—Photomicrographs of primary bioclastic composition of rudstones and grainstones and diagenetic features: **A**) poorly sorted bivalve rudstone with intraparticle porosity (plane-polarized light, PL). **B**) Neomorphosed gastropod cemented by interparticle and intraparticle pore-lining particle and discrete intraparticle laterite calcite (PL). **C**) Grainstone composed mainly of ostracods (red arrow). Molds of dissolved bioclasts impregnated by blue epoxy resin (yellow arrow) (PL). **D**) Rudstone composed of neomorphosed bivalves with interparticle fine rim of pore-lining calcite (red arrow); black arrow indicates thin lines from original texture of bivalve shell (PL). **E**) Rudstone with dissolved bivalve molds surrounded by thin micrite envelope (blue arrow) cemented by drusy calcite on both moldic (black arrow) and interparticle porosity (red arrow) (PL). **F**) CL photomicrograph showing neomorphosed bivalves (red arrow) with dull CL; interparticle pores (blue arrow shows porosity) lined by calcite rims (white arrow) and partially cemented by fine mosaic calcite (red luminescence) (cathodoluminescence, CL).

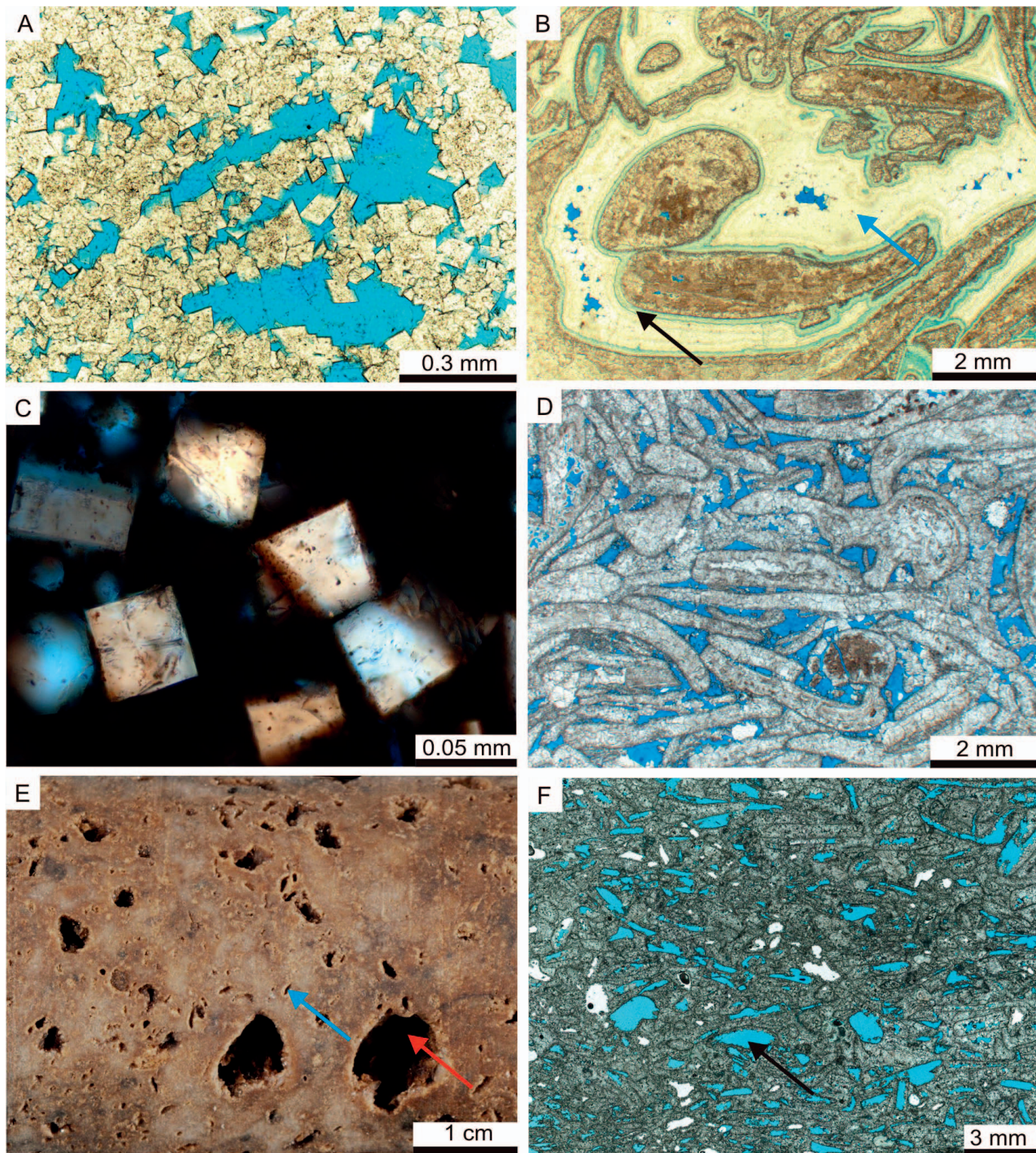


FIG. 4.—Common aspects of diagenesis and porosity from bivalve rudstones and grainstones: **A**) sucrosic dolostone with some molds of dissolved bioclasts (PL). **B**) Bivalve rudstone cemented by displacive silica (blue arrow). Pale green rim is microporous silica impregnated by blue epoxy resin (black arrow) (PL). **C**) Svanbergite crystals replacing mud intraclast (crossed-polarized light, XPL). **D**) Bivalve rudstone cemented by thin pore-lining calcite with preserved interparticle porosity. Bioclasts partially neomorphosed, partially dissolved, and further cemented by calcite mosaic (PL). **E**) Core photograph showing vugs (red arrow) and molds (blue arrow) in bivalve rudstone. **F**) Moldic porosity (black arrow) in bivalve grainstone. Interparticle and part of moldic porosity occluded by calcite cement (PL).

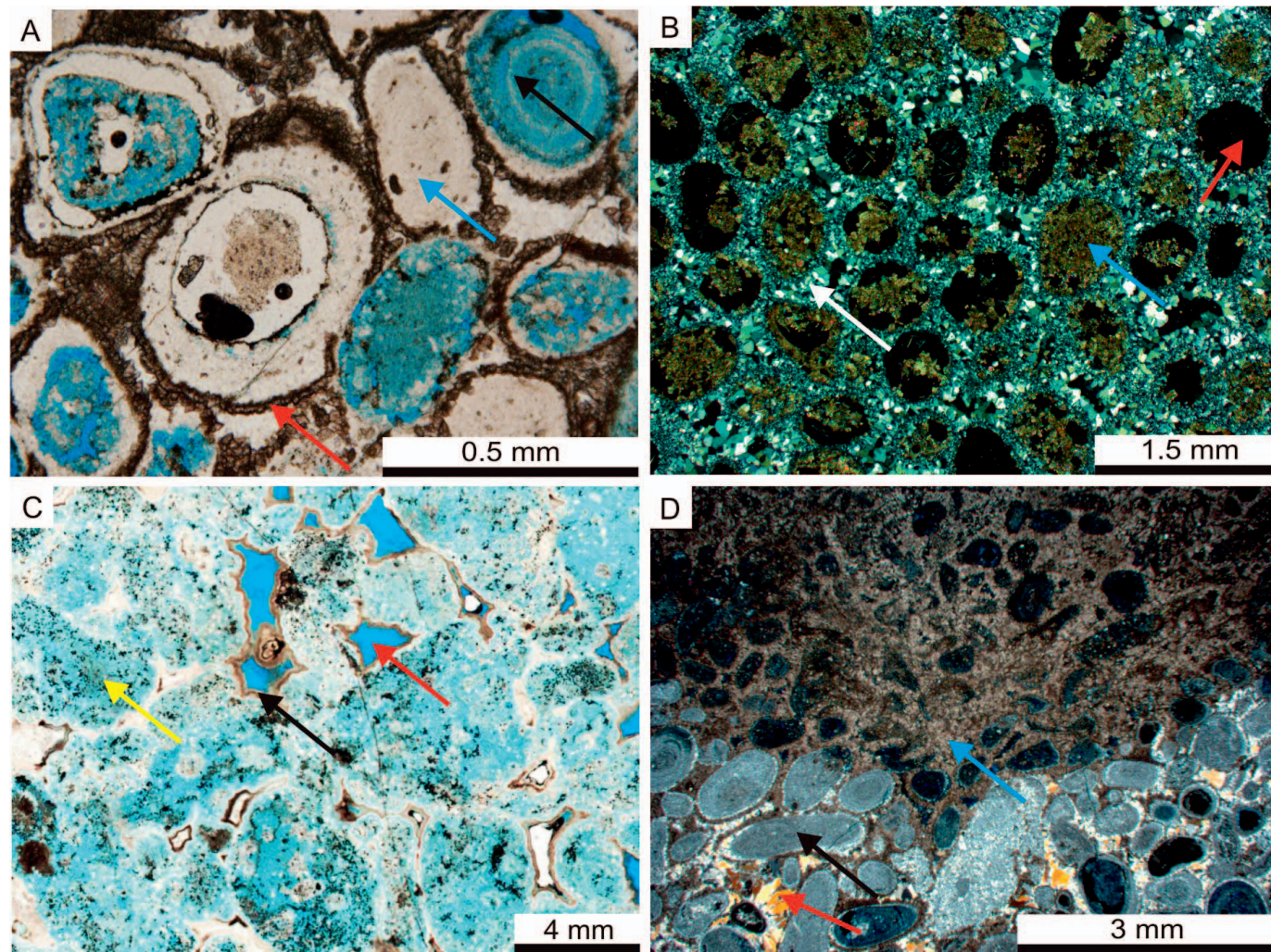


Fig. 5.—Optical photomicrographs showing highly heterogeneous imprint of diagenesis on stevensitic arenites: **A**) partially dissolved stevensitic ooids (black arrow), replaced by silica (blue arrow) and covered by dolomite rim (red arrow) (PL). **B**) Partially dissolved ooids (red arrow), replaced by dolomite (blue arrow) and cemented by chalcedony rim and quartz mosaic (white arrow) (XPL). **C**) Microporous chert (yellow arrow) replacing stevensitic arenite with remnants of primary porosity (red arrow). Microporosity is impregnated by blue epoxy resin, resulting in a pale blue color. Black arrow indicates oil inclusions in microporosity (PL). **D**) Contact between mostly silicified stevensite arenite (black arrow) and dolomitized arenite (blue arrow). Red arrow shows prismatic quartz filling interparticle porosity (XPL).

dolomitized, and/or dissolved (Fig. 5A). Calcite is rare in the stevensitic arenites, occurring mainly as coarse mosaic fracture-filling cement.

Authigenic silica lines ooids as fibrous and microcrystalline rims, followed by pore-filling fine- to coarse-crystalline, drusy mosaic (Fig. 5B). Partial to total replacement of ooids by microcrystalline silica is frequent (Fig. 5C, D). Microcrystalline silica, as botryoidal or drusy aggregates, fills vugular, interparticle, and fracture pores. Botryoidal chalcedony has small brown inclusions and green to blue UV fluorescence. Microcrystalline silica has abundant microporosity and fracturing.

Blocky or mosaic dolomite replaces ooids (Figs. 5B), and drusy dolomite fills interparticle porosity, and occurs as pore-lining rims (Fig. 5A, D). In some cases, dolomite occurs only selectively replacing the ooids, while in other cases it occurs only filling the interparticle pores. Pervasive dolomitization, mimetic or totally fabric obliterative, is common. Rarely, saddle dolomite replaces diagenetic silica. CL images indicate zoned red luminescence patterns on dolomite crystals. Dolomite fluoresces dark to light blue, and light green under UV. Millimetric to centimetric levels of pervasively dolomitized or silicified arenites occur intercalated,

through stylolitic contacts, heterogeneously organized. Traces of fluorite, svanbergite–goyazite, and pyrite occur replacing silica.

Moldic and intraparticle porosity due to dissolution of ooids (Figs. 5A) and intercrystalline porosity due to dolomitization are the most common pore types in stevensitic arenites. Interparticle porosity is reduced by cementation and compaction, but remnants of primary porosity were observed in a few samples (Fig. 5C). Silicified arenites have significant microporosity (Fig. 5C) and localized vugs.

Stevensitic Claystones with Calcite Spherulites.—The deposits of magnesian clays of the sag section were often replaced by calcite spherulites (Fig. 6A), dolomite, and silica. Due to chemical instability of the Mg-clays, their original fabric is difficult to identify. These clay deposits are more abundant in Well 4, where they are preserved in an interval about one hundred meters thick. In the other wells, Mg-clay deposits were extensively replaced. Mg-clays are pale to dark brown in uncrossed polarizers, occurring as laminated or massive aggregates (Fig. 6B), as peloids with very variable size (Fig. 6C), as ooids with up to 2 mm of diameter, as thin coatings covering intraclasts (Fig. 6D), as

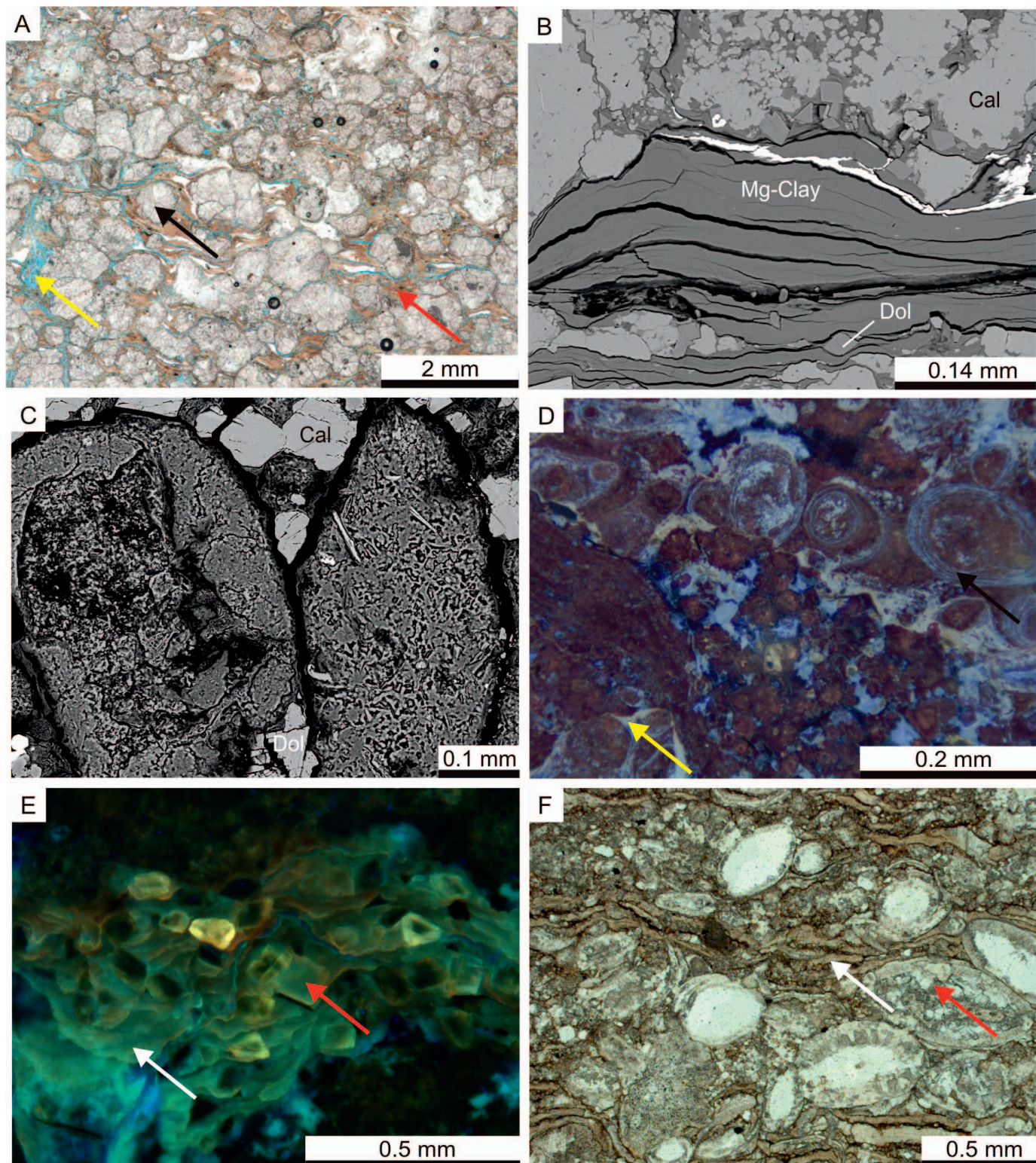


FIG. 6.—Important characteristics of stevensitic claystones: **A**) shrunken and partially dissolved (yellow arrow) stevensite laminations (red arrow) replaced by recrystallized calcite spherulites (black arrow) (PL). **B**) Slightly shrunken stevensite (Mg-clay) laminated aggregates, partially replaced by dolomite (Dol) and calcite (Cal) (backscattered electrons image, BSE). **C**) Stevensite ooid-peloid. Ooid on the left has a partially dissolved nucleus and an outer massive texture, whereas peloid on the right has a dominantly massive texture (BSE). **D**) Stevensite as ooids (black arrow) and as coatings (yellow arrow) on intraclasts (ultra-violet fluorescence, UVF). **E**) Laminated stevensite aggregates (white arrow) partially replaced by dolomite (red arrow) (UVF). **F**) Articulated ostracod bioclast shells (red arrow) filled and replaced by quartz in deformed stevensite laminations replaced by mimetic dolomite (white arrow) (PL).

pseudomatrix, and as matrix in hybrid siltstones and in intraclastic packstones. Laminated and massive aggregates often show shrinkage cracks. Clay peloids and ooids are often deformed. Even when partially dissolved or replaced by carbonates or silica, clay particles and laminated aggregates are blue, yellow, and light brown to orange UV fluorescent (Fig. 6D, E). SEM analyses show poor crystallinity, even at high magnification. Semiquantitative EDS analyses indicate considerable amounts of SiO_2 (about 65%) and MgO (about 30%), and low contents of Al_2O_3 (about 2%). FeO , K_2O , CaO , and NaO_2 occur in amounts below 1%. The elemental composition of the clays and their XRD analysis indicate that the dominant mineral is stevensite.

Silt- to sand-size siliciclastic grains are sparsely mixed with the stevensite deposits, usually in less than 1%. Hybrid sandstones and siltstones with quartz, biotite, muscovite, orthoclase, and plagioclase grains are rare. Hybrid siltstones are particularly abundant at the base of the sag section in Well 2, within an interval about 100 meters thick and at the top of the sag section in all wells (Fig. 2). Phosphatic bioclasts, such as fish scales, teeth, vertebrae, and other bones, occur scattered or concentrated, being common in Well 1, locally together with other phosphatic grains. Ostracods are frequently concentrated in the laminations (Fig. 6F), and occur articulated, with limited reworking. Their partial to total replacement by quartz or dolomite is common (in 34% of samples).

Calcite spherulites are the most common diagenetic constituent in the stevensite deposits, occurring as an important component in all studied wells (Figs. 6A, 7A, B). Spherulites 0.15 to 2.5 mm in diameter (average = 0.8 mm) frequently replaced the stevensitic claystones and hybrid siltstones, displacing and deforming the unconsolidated sediments (Figs. 6A, 7B). Few spherulites have recognizable nuclei made of clay peloids, ostracods, intraclasts, and lumps of microcrystalline calcite. Spherulites are abundant, coalescing as irregular levels (Fig. 7B), sutured by microstylolites. Although the spherulites were recrystallized, resulting in changes in crystal shape and size, many have good preservation of the original fibrous structure (Fig. 7A, C). Partial replacement of the spherulites by chalcedony and quartz is frequent (31% of the samples).

Spherical to subspherical low-magnesium calcite pisoliths (1 mm to 5 cm) are abundant in Well 1 (Fig. 2), showing fascicular-optic and/or radial-fibrous texture, similar to crusts, but with concentric growth (Fig. 7D). Some pisoliths are formed by thin concentric laminae (~0.5 mm), while others are formed by divergent coalescence of fascicular-optic calcite aggregates, reaching up to 2 mm in diameter. The pisoliths are deformed and recrystallized. Pisolithic aggregates are not fluorescent and seem to replace stevensite like spherulites inside unconsolidated sediments.

Dolomite replaces stevensite in nearly all the samples (Figs. 6B, E, F, 7A, B). Stevensite laminae are replaced and deformed by blocky dolomite (Figs. 6B, 7A). Saddle dolomite replaces the primary and diagenetic constituents in 12% of the samples. Dolomite frequently totally replaces the stevensite and calcite spherulites. In the hybrid siltstones, authigenic illite-smectite clays are identified in XRD. Intercalations of millimetric to centimetric levels of cherts and dolostones, along stylolitic contacts, are formed by replacement of laminated clay deposits. Dolomite fluoresces blue, green, yellow, or brown under UVF (Fig. 6E), while silica is brown to green under UVF when replacing stevensite.

Cubic, blocky, and microcrystalline pyrite, although scarce (< 1%), occurs in most of the described thin sections, mainly replacing the stevensite and other primary or diagenetic constituents. Pseudocubic, microcrystalline svanbergite-goyazite ($\text{SrAl}_3(\text{PO}_4/\text{SO}_4)(\text{OH})_6$ / $\text{SrHAl}_3(\text{PO}_4)_2(\text{OH})_6$) are recognized in SEM analyses, associated with silicification and dolomitization.

Partial to total dissolution of stevensite is very common (Fig. 7E, F). Microporosity is observed both by NMR (nuclear magnetic resonance) and SEM analyses in preserved stevensite deposits.

Fascicular Calcite Crusts.—Non-magnesian calcite crusts of radial-fibrous and more commonly fascicular-optic crystal aggregates (sensu Kendall 1977; i.e., plumose or increasingly divergent) constitute the main reservoirs of the sag section. These calcite aggregates grew predominantly in a vertical to near vertical orientation (Fig. 8A, B), with an average individual length of 1.55 mm (up to 12 mm), encrusting various deposits. The fascicular aggregates commonly display a shrub shape that coalesces both vertically and horizontally, forming calcite crusts of variable thickness, up to 80 cm thick. In some cases, fibrous calcite aggregates form millimetric continuous and isopachous palisade crusts (Fig. 8C), intercalated with microcrystalline calcite or dolomite, siliciclastic mud, or stevensite laminae. Recrystallization is frequent, generating apparently massive forms, although with remnants of the original fibrous crystal fabric recognizable in polarized light and in SEM images (Fig. 8D). The engulfment and replacement of siliciclastic grains, stevensite peloids, and ostracod bioclasts by fascicular-optic calcite aggregates is common. In some cases, thin laminations occur within the aggregates. CL images show a homogeneous red luminescence pattern (Fig. 9A), and UVF is very weak or absent. Microbial remnants were not identified in SEM analyses.

Dolomite is the most common diagenetic constituent filling interstitial growth-framework pores in calcite crusts (78% of the samples; Fig. 9B, C), with blocky, microcrystalline and more rarely mosaic habits. Saddle dolomite occurs filling growth-framework and vugular porosity, as well as replacing the primary and diagenetic constituents. Partial to total dolomitization of the original deposits is common, in some cases mimetic (Fig. 9D), and in other cases destroying the original fabrics. Dolomite shows red-zonation CL patterns. Calcite fills the growth-framework porosity in 31% of the samples. Rarely, calcite rims of scalenohedral, prismatic, and bladed crystals cover calcite fascicular aggregates (6% of the samples). Partial or total recrystallization of fascicular aggregates to microcrystalline calcite is common. Authigenic fibrous and microcrystalline silica selectively replaces fascicular calcite crusts in 92% of the samples (Figs. 9A, B, E) and fills growth-framework porosity in 42% of the samples. Pervasive replacement by microcrystalline silica commonly promotes the formation of microporosity and/or vugular porosity. Coarse mosaic or prismatic quartz locally replaces the fascicular aggregates and fills the growth-framework porosity.

Coarse mosaic, prismatic, or radial-fibrous barite and celestine were described in 11% of the samples, filling fractures or growth-framework porosity (Fig. 9C). Authigenic non-magnesian clay minerals are not significant in volume, but occur very frequently in the studied samples. Illite, illite-smectite, and kaolinite clays identified in SEM (Fig. 9F) and XRD, occur in the calcite crusts, mainly replacing detrital interstitial components.

Growth-framework porosity in the interstices among coalescent fascicular calcite aggregates constitutes the main type of primary porosity in calcite crusts (Fig. 8A). These pores are enlarged by dissolution of the aggregates (Figs. 8A, 9B, C). Dolomite cement is the main reducer of growth-framework porosity (Figs. 9B). Compaction does not significantly affect growth-framework porosity. Intracrystalline porosity in calcite crust and dolomite crystals that filled growth-framework porosity is common (Figs. 9B, C, E).

Intraclastic Grainstones, Rudstones, and Clay-Rich Packstones.—Massive intraclastic grainstones and rudstones, composed of fragments of reworked calcite crusts, stevensitic claystones intraclasts and particles, calcite spherulites, laminated microbial carbonates, and microcrystalline calcite peloids are common (Fig. 10A–D). The average diameter of such particles is 1.56 mm (up to 25 mm). Calcite intraclasts are commonly rounded, with shapes controlled either by their internal crystal habit or by their laminated fabrics. Mg-clay matrix is a common constituent in intraclastic rocks (Fig. 10B). Rocks with this combined composition were termed clay-rich packstones (or hybrid “packstones”).

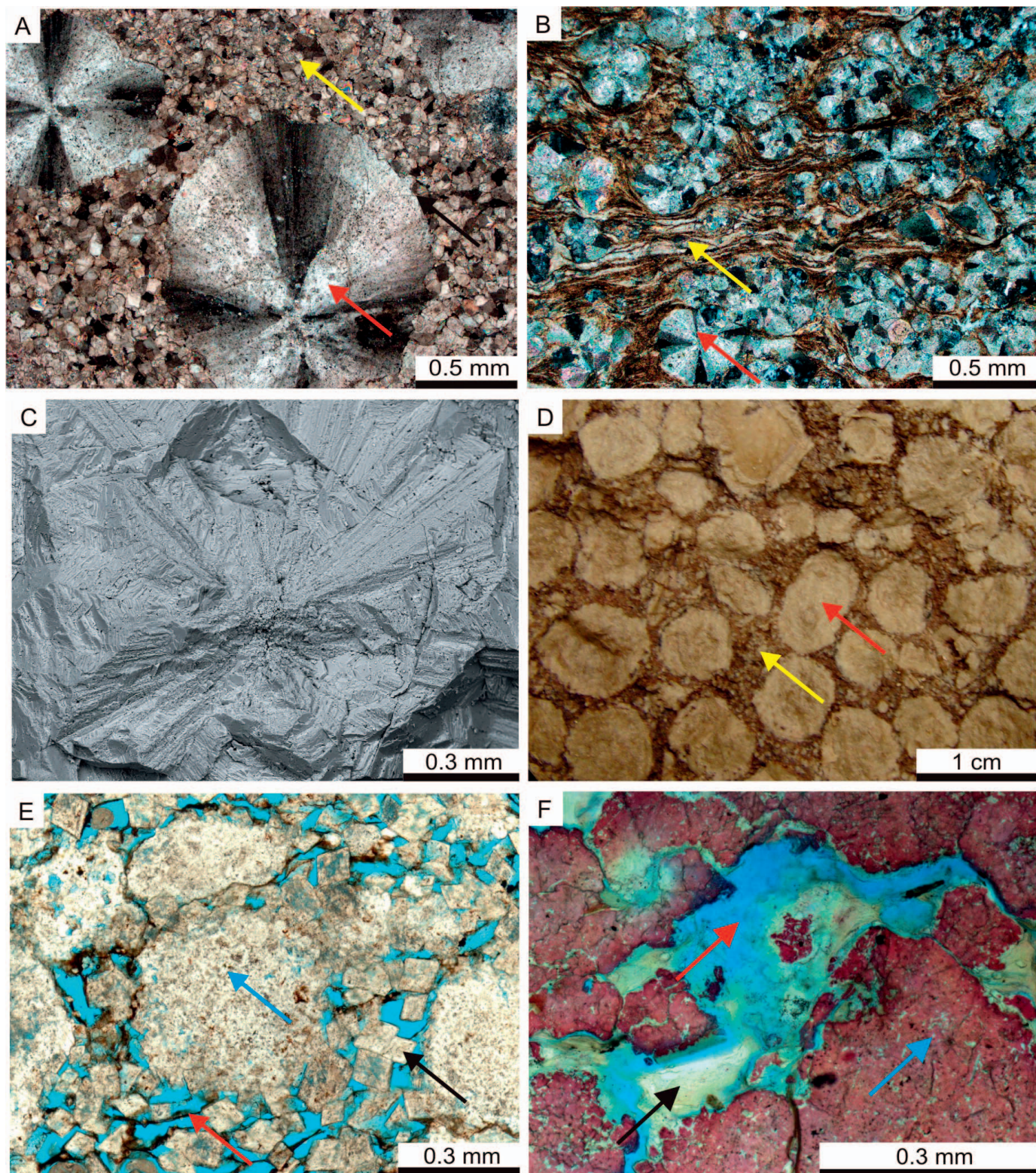


FIG. 7.—Aspects related to replacement and dissolution of stevensitic claystones. **A**) Slightly silicified spherulites (red arrow) in a clay matrix replaced by dolomite (yellow arrow) (XPL). **B**) Partially silicified spherulites (red arrow), displacing and replacing clay laminae (yellow arrow). Dolomite is interpreted as a result of mimetic replacement of stevensite (XPL). **C**) Radial-fibrous structure of a calcite spherulite, interpreted as original (secondary electrons image, SEI). **D**) Core photograph of calcite pisoids (red arrow) replacing stevensite further replaced by dolomite (yellow arrow). **E**) Matrix dissolution porosity (blue epoxy resin) among dolomite rhombs (black arrow) and calcite spherulites (blue arrow). Lamination marked by undissolved brown organic matter lines (red arrow). Note, also, partial dissolution of calcite spherulites (PL). **F**) Partially dissolved (red arrow) magnesian clay (black arrow), replaced by calcite (blue arrow) (stained with acid solution of alizarin red and potassium ferrocyanide) (PL).

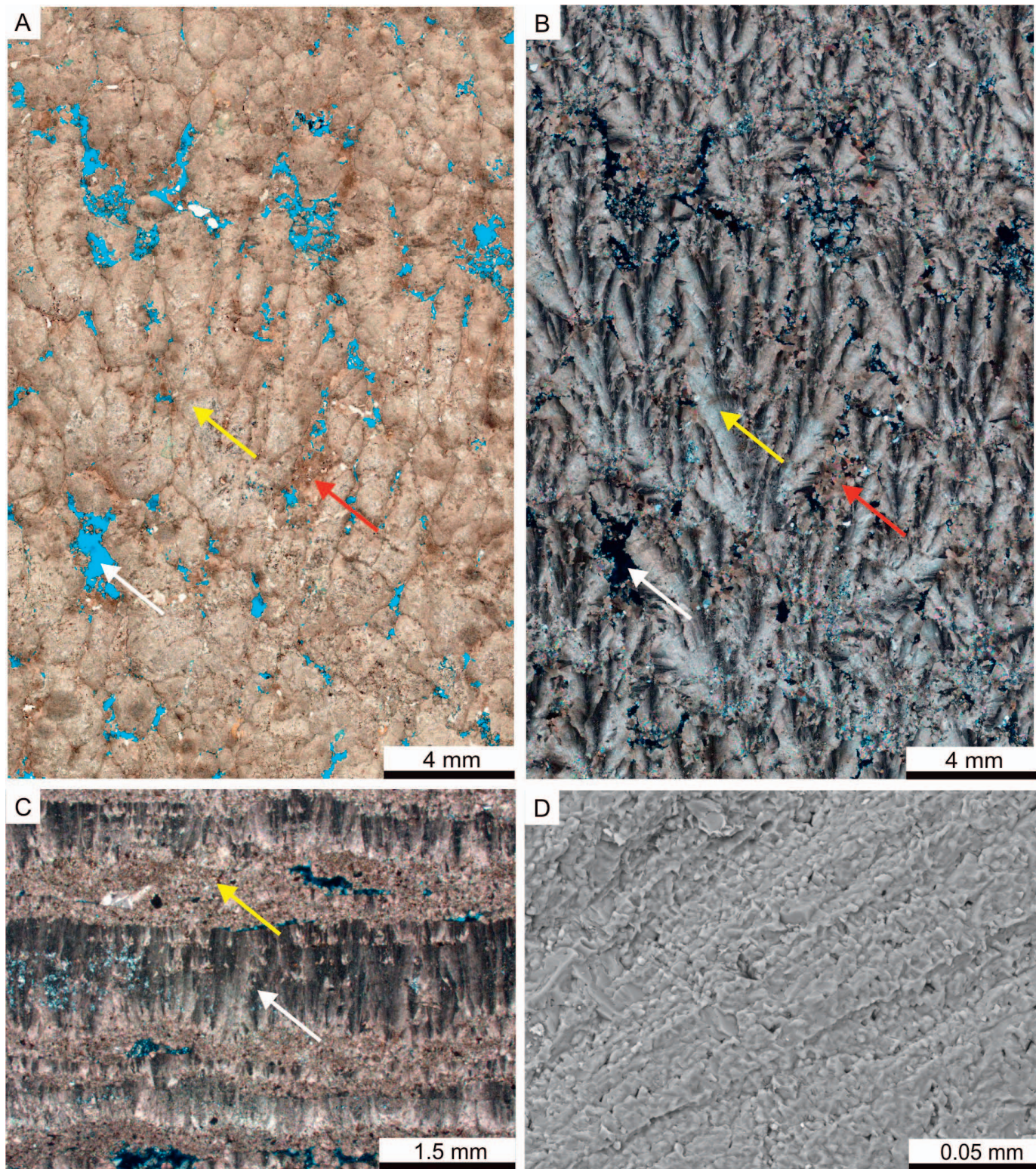


FIG. 8.—Aspects of fascicular-optic calcite crusts: A, B) divergent crystal aggregate optic axes with fascicular-optic texture (yellow arrow), growth-framework pore enlarged by dissolution (white arrow), and dolomite pore filling (PL, XPL). C) Isopachous fibrous fascicular-optic calcite palisade crusts (white arrow) intercalated with replacive dolomite (yellow arrow) (XPL). D) Detail of the mimetic recrystallization of fibrous calcite, showing significant amount of micropores (SEI).

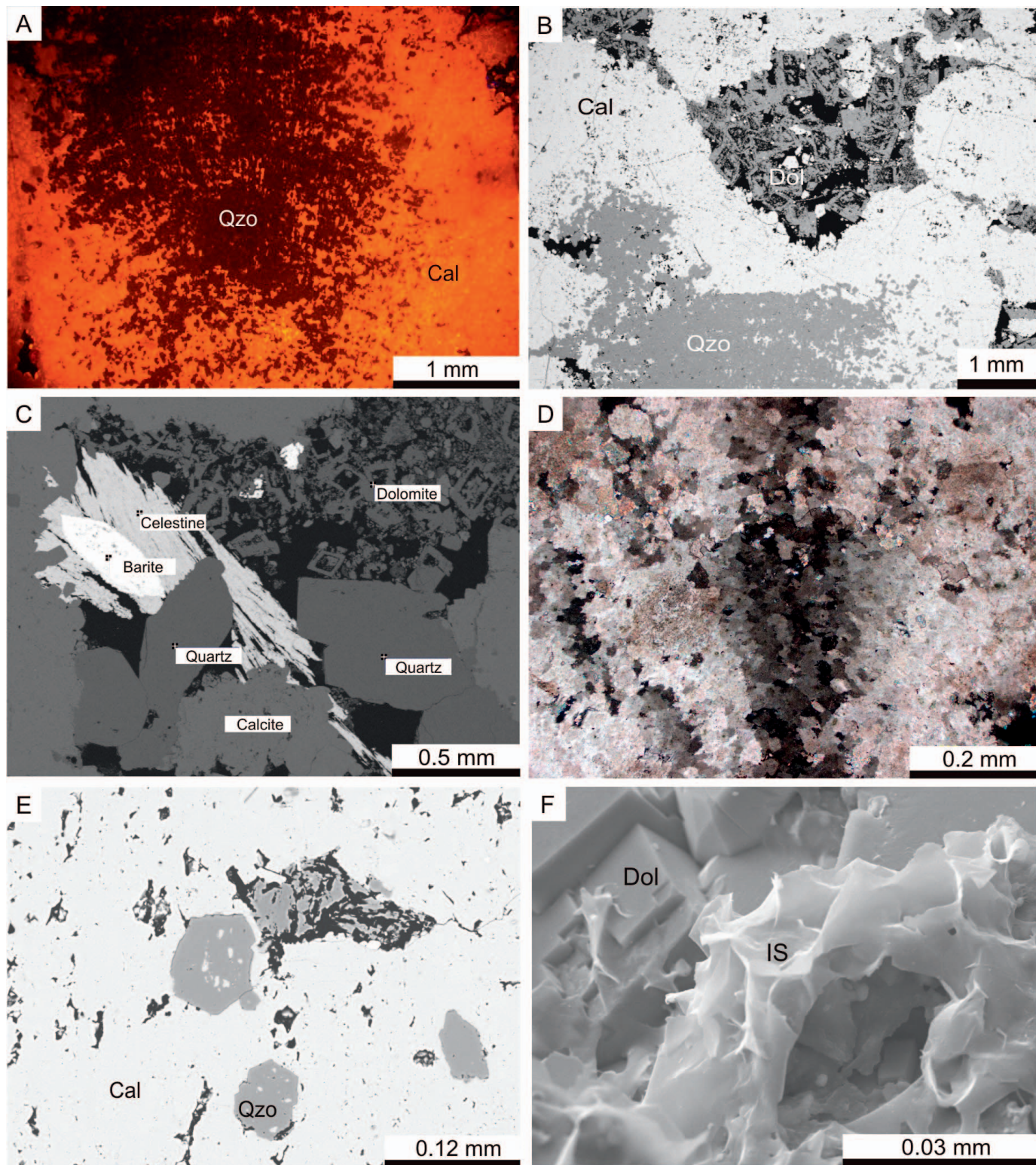


FIG. 9.—Detail of diagenetic modifications of fascicular-optic calcite crust: **A**) calcite (Cal) shrub with massive recrystallization and replacement by quartz (Qzo). Note the homogeneous luminescence pattern in calcite (CL). **B**) Calcite (Cal) crust partially replaced by microcrystalline quartz (Qzo) and with growth-framework porosity partially cemented by zoned dolomite (Dol). Dolomite exhibits intracrystalline dissolution. (BSE). **C**) Quartz, celestine, barite, and dolomite filling growth-framework enlarged porosity and replacing calcite crust. Note partial dissolution of dolomite rhombs (BSE). **D**) Dolomite mosaic replacing fascicular-optic calcite (XPL). **E**) Detail of the internal structure of a fascicular-optic calcite (Cal) aggregate, replaced by quartz (Qzo) and showing abundant intracrystalline porosity (BSE). **F**) Illite-smectite (IS) covering dolomite (Dol) filling growth-framework porosity (SEI).

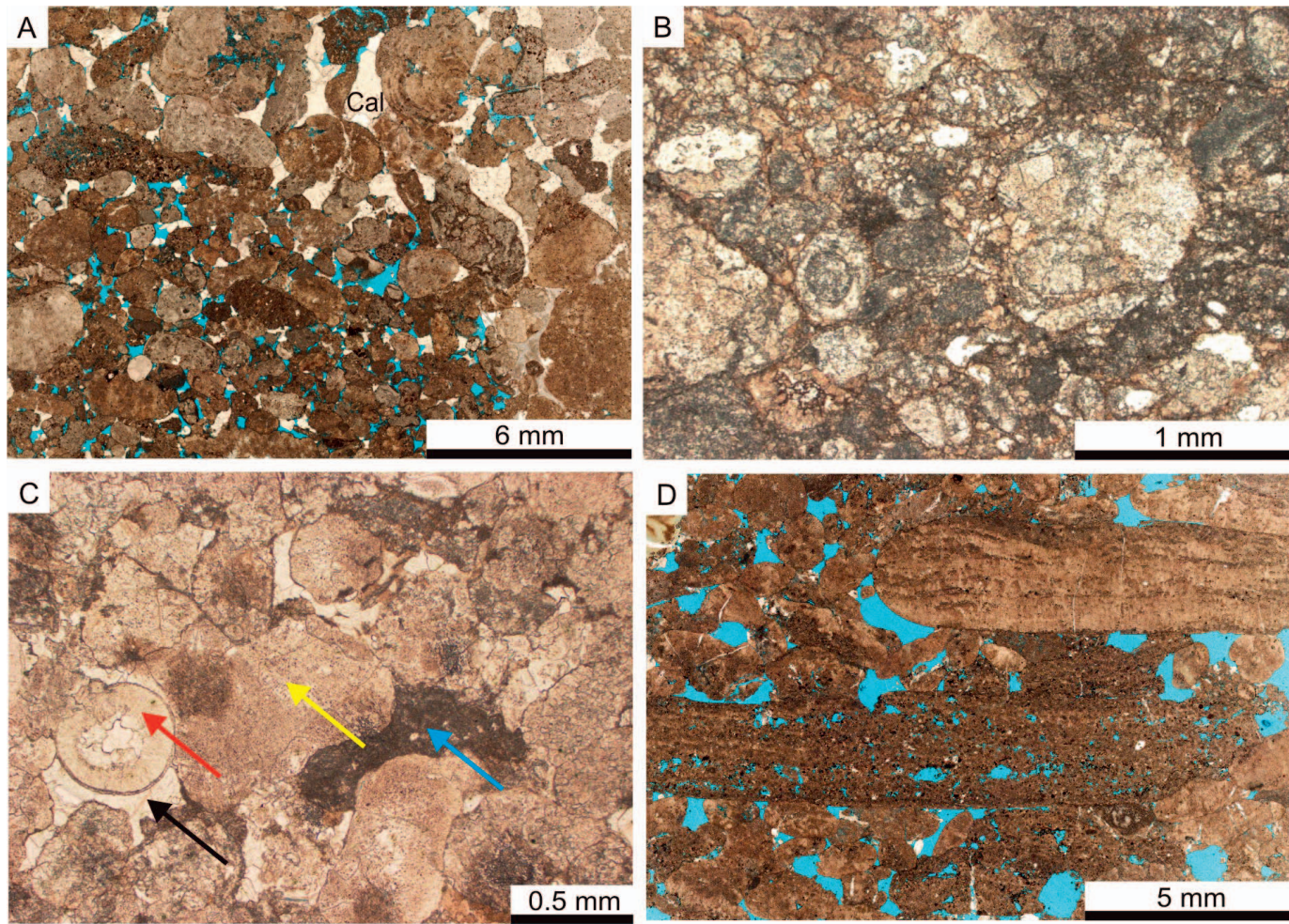


FIG. 10.—Aspects of intraclastic rocks: **A**) intraclastic rudstones partially cemented by calcite (Cal) (PL). **B**) Clay-rich packstone composed of carbonate intraclasts in a clay matrix (PL). **C**) Intraclastic grainstone composed of calcite spherulites (red arrow), fragments of fascicular-optic calcite (yellow arrow), and microcrystalline calcitic intraclasts (blue arrow), cemented by calcite (black arrow) (PL). **D**) Intraclastic rudstone with primary interparticle porosity and secondary porosity generated by particle dissolution (impregnated with blue epoxy resin) (PL).

Dolomite fills interparticle pores in 81% of the samples of intraclastic grainstones and rudstones. Saddle dolomite is a common interparticle cement. Blocky, microcrystalline, and/or coarse mosaic calcite occurs as cement filling interparticle pores in 100% of the samples (Fig. 10A). Calcite rims of scalenohedral, prismatic, and bladed crystals cover the intraclasts in 25% of the samples. Silica replaces carbonate intraclasts in 62% of the samples. Coarse mosaic or prismatic quartz occasionally replaces intraclastic grainstones (19% of the samples).

Mechanical compaction of the intraclastic rocks revealed by grain fracturing and deformation, and chemical compaction through pressure dissolution along interparticle contacts or stylolites is frequently intense. Porosity enhancement by particle dissolution is frequent (Fig. 10D). Primary interparticle and secondary moldic porosity are reduced by mechanical and chemical compaction and by cementation (Fig. 10C).

Processes Related to Faults and Fractures.—Alterations associated with faults and fractures affect various facies and occur more expressively in an interval approximately 10 m thick in well 2 (Fig. 11A), just above the unconformity separating the rift stage from the sag stage. Fractures occur open or filled with quartz, calcite, dolomite, celestine, and/or other minerals, such as pyrite, barite, anhydrite, kaolinite, fluorite, and sphalerite. These alterations generate highly complex and heterogeneous textures,

often brecciated and dominated by the precipitation of dolomite (up to 100% of volume) and quartz (Fig. 11B). Fine idiopatic dolomite (around 50 μm) and saddle dolomite (Fig. 11C) crystals are dominant, frequently dissolved or broken. Prismatic quartz replaces and engulfs dolomite (up to 35% of volume). Celestine occurs as small prismatic or fibrous crystals filling fractures and replacing dolomite (Fig. 11D). Coarse calcite fracture filling was observed in one sample. Traces of svanbergite–goyazite pseudocubic crystals occur replacing dolomites (Fig. 11E). Fault- and fracture-related alteration generated highly porous dolostones with intercrystalline porosity enlarged by dolomite dissolution (Fig. 11F) and with porosity enhanced by open fractures.

Porosity, Permeability, and Mercury Injection Capillary Pressure (MICP)

The overall porosity ranges between 0.1 and 37% (average = 7.67%), and the average permeability is 16.241 mD (maximum = 1193 mD). About 40% of the samples are not considered reservoirs, including stenositic claystones, hybrid siltstones, microbial laminites, pisolithic rudstones, clay-rich packstones, cherts, and sparites, which usually have low porosities and permeabilities (< 0.001 mD). Table 1 summarizes basic petrophysical results of the main rock types. Pore throat sizes obtained

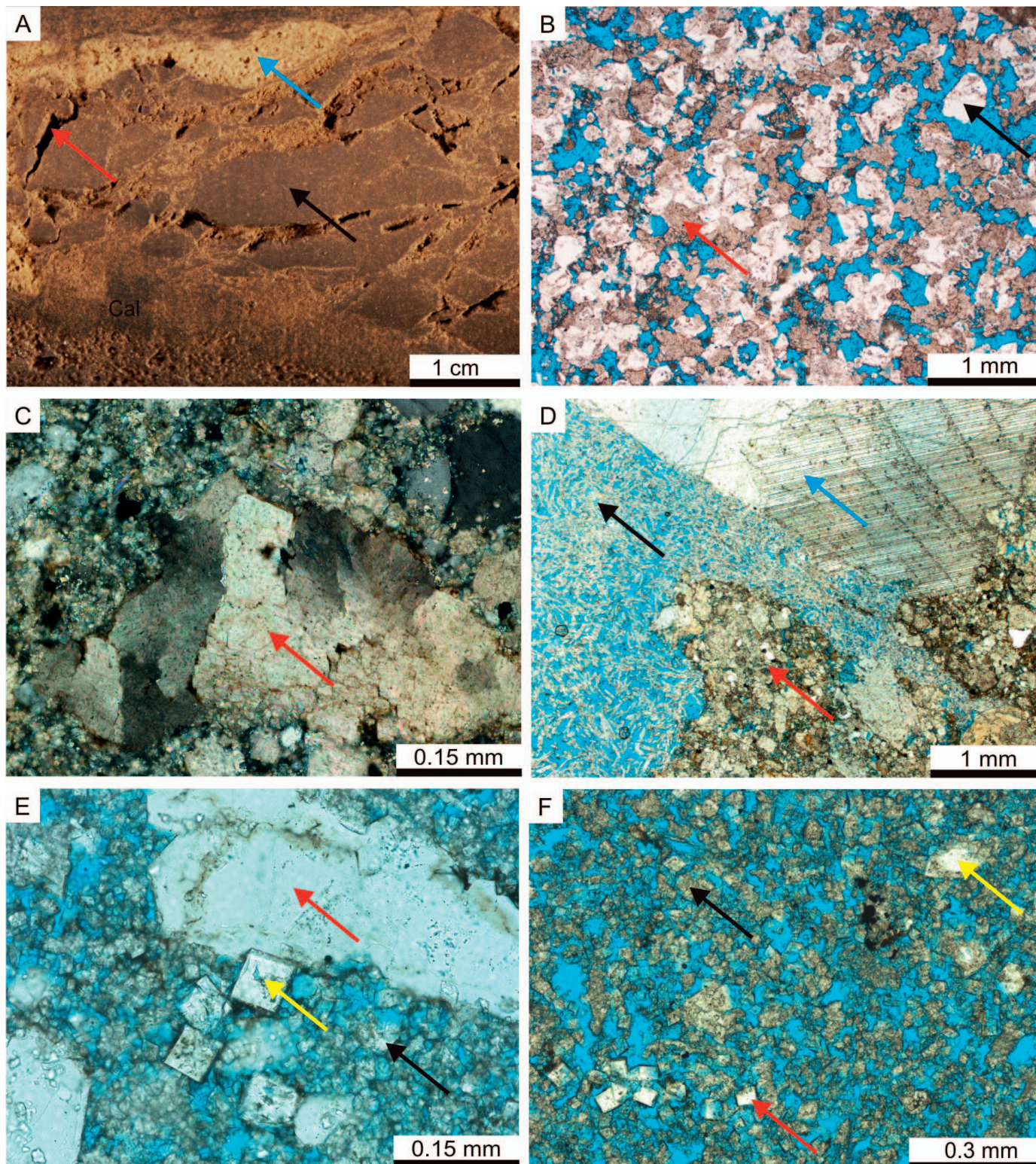


FIG. 11.—Aspects of alteration related to fracturing: **A**) core photograph of semi-consolidated brecciated dolostone with centimetric clasts (black arrow), open fractures (red arrow), and fractures filled by celestine (blue arrow). **B**) Partially dissolved saddle dolomite (red arrow), partially replaced and engulfed by quartz crystals (black arrow) (PL). **C**) Saddle dolomite (red arrow) within cataclastic fabric partially replaced by quartz (XPL). **D**) Celestine (black arrow) and calcite (blue arrow) filling fractures in brecciated dolostone (red arrow) (PL). **E**) Prismatic quartz (red arrow) and svanbergite–goyazite pseudocubic crystals (yellow arrow) replacing cataclastic dolomite (PL). **F**) Small fractured dolomite rhombs (black arrow) replaced by quartz (red arrow) and svanbergite (yellow arrow). Intercrystalline porosity impregnated by blue epoxy resin (PL).

TABLE 1.—Statistical summary of petrophysical analysis, showing the parameters of porosity and permeability of main defined petrofacies.

Petrofacies	Bioclastic Rudstones						Bioclastic Grainstones		Stevensitic Arenites	
	Interparticle		Moldic		Vug		Moldic		Multiple Types	
Predominant Pore Type	Ø (%)	k (mD)	Ø (%)	k (mD)	Ø (%)	k (mD)	Ø (%)	k (mD)	Ø (%)	k (mD)
Average	8.68	7.209	10.32	1.055	7.91	0.142	14.46	1.540	18.74	21.400
Median	8.60	1.760	9.60	0.198	7.20	0.078	14.65	0.561	17.95	0.432
Standard Deviation	2.34	15.348	4.27	2.427	2.85	0.185	3.21	1.961	7.22	62.825
Variance	5.46	235.548	18.20	5.888	8.13	0.034	10.28	3.846	52.18	3947.036
Kurtosis	1.10	13.235	4.58	11.087	1.58	4.024	-0.81	1.006	-0.57	15.983
Range	12.80	74.699	20.70	10.299	12.30	0.759	11.40	5.951	26.10	266.999
Minimum	1.80	< 0.001	5.10	< 0.001	2.80	< 0.001	8.50	0.019	5.10	< 0.001
Maximum	14.60	74.700	25.80	10.300	15.10	0.760	19.90	5.970	31.20	267.000
n	45	45	31	31	27	27	18	18	18	18
Petrofacies	Coalescent Crust		Non Coalescent Crust		Intraclastic Rocks		Dolostones			
	Growth-framework		Intercrystalline		Interparticle		Intercrystalline		All Samples	
Predominant Pore Type	Ø (%)	k (mD)	Ø (%)	k (mD)	Ø (%)	k (mD)	Ø (%)	k (mD)	Ø (%)	k (mD)
Average	6.85	28.937	6.14	0.809	6.34	10.445	15.80	111.040	7.67	16.241
Median	7.00	0.435	5.50	0.055	6.00	0.010	15.55	32.000	6.80	0.074
Standard Deviation	4.09	64.646	3.47	2.400	4.68	61.224	7.43	229.450	5.76	77.137
Variance	16.69	4179.164	12.07	5.759	21.91	3748.384	55.19	52647.488	33.14	5950.070
Kurtosis	-1.25	6.818	-1.14	28.798	-0.57	66.974	-0.31	15.590	2.77	124.215
Range	15.90	294.999	12.30	16.199	18.90	522.999	31.10	1192.999	36.90	1192.999
Minimum	0.20	< 0.001	1.30	< 0.001	0.10	< 0.001	1.30	< 0.001	0.10	< 0.001
Maximum	16.10	295.000	13.60	16.200	19.00	523.000	32.40	1193.000	37.00	1193.000
n	105	105	67	67	77	77	40	40	599	599

through MICP analyses were classified according to the Hassall et al. (2004) classification (micro pores: pore throats less than 0.5 μm ; meso pores: pore throats between 0.5 μm and 5 μm ; macro pores: pore throats more than 5 μm). The average pore throat is 4.92 μm (median = 3.03 μm), and the distribution of pore sizes shows slight predominance of mesoporosity (micro = 33.19%; meso = 39.08%; macro = 27.73%).

Bioclastic Rudstones.—The permeability of bioclastic rudstones varies significantly according to the predominant type of porosity. The porosity of rudstones with predominance of interparticle porosity varies between 1.8 and 14.6% (average = 8.68%) and average permeability is 7.2 mD (maximum = 74.7 mD). Rudstones with predominant moldic and intraparticle porosity have higher porosities than those with predominantly interparticle porosity (average = 10.32%; 5.1–25.8%), but lower permeability (average = 1.1 mD; < 0.001–10.3 mD). Rudstones with predominant vugular porosity have the lowest permeability and porosity values (average = 7.91%; 2.8–15.1%; average permeability = 0.14 mD; < 0.001–0.76 mD). MICP analyses of bioclastic rudstones and grainstones showed average pore throats of 4.92 μm (median = 3.77 μm) with multiple modes, reflecting the heterogeneity of the porous system. The distribution of pore sizes shows predominance of microporosity (micro = 47.1%; meso = 28.7%; macro = 24.2%).

Bioclastic Grainstones.—The porosity of bioclastic grainstones ranges between 8.5% and 19.9% (average = 14.46%) and their average permeability is 1.54 mD (0.019–5.97 mD). Mesoporosity largely predominates (micro = 20.85%; meso = 60.65%; macro = 18.50%), with average pore throat of 3.25 μm (median = 2.33 μm).

Stevensitic Arenites.—Stevensitic arenites have significant variability in porous types, as previously described, which corresponds to the large

variation in porosity and permeability. Their porosity varies between 5.1 and 31.2% (average = 18.74 %), and the average permeability is 21.4 mD (< 0.001–267 mD). MICP showed average pore throat of 6.02 μm (median = 2.87 μm). The distribution of pore sizes shows predominance of macroporosity (micro = 29.05%; meso = 28.50%; macro = 42.55%).

Coalescent Fascicular Calcite Crusts.—Well-developed coalescent calcite crusts have porosities ranging between 0.20 and 16.10% (average = 6.85%) and average permeability of 28.94 mD (< 0.001–295 mD). MICP showed average pore throat of 7.77 μm (median = 4.31 μm). The distribution of pore sizes shows predominance of microporosity (micro = 37.50%; meso = 31.00%; macro = 31.50%).

Non-Coalescent Fascicular Calcite Crusts.—Poorly developed non-coalescent crusts, with porosity dominantly developed by stevensite dissolution, have porosity between 1.30 and 13.6% (average = 6.14%) and average permeability of 0.8 mD (< 0.001–16.2 mD). Microporosity predominates (micro = 50.94%; meso = 40.49%; macro = 8.57%), with average pore throat of 1.96 μm (median = 0.64 μm).

Intraclastic Grainstones, Rudstones, and Clay-Rich Packstones.—Intraclastic grainstones and rudstones have average porosities of 6.34% (0.1–19%) and average permeability of 10.45 mD (< 0.001–523 mD). **Dolostones.**—Dolostones have the highest porosity and permeability among the recognized rock types, with porosity ranging between 1.3 and 32.4% (average = 15.80%) and maximum permeability reaching 1193 mD (average = 111.04 mD). MICP showed average pore throat of 5.59 μm (median = 4.27 μm). The distribution of pore sizes shows predominance of mesoporosity (micro = 13.67%; meso = 45.17%; macro = 42.16%).

DISCUSSION

Eogenetic Evolution of Bivalve–Gastropod Rudstones and Grainstones

Most of the diagenesis of the bioclastic rocks occurred before compaction (Fig. 12), as evidenced by the distribution of the blocky and drusiform interparticle pore-filling cements. The bioclastic rocks followed three main evolution pathways, controlled by distinct eogenetic conditions (Fig. 13). Pathway 1 was probably connected to active circulation of interstitial fluids undersaturated with respect to aragonite, most likely lacustrine freshwaters during more humid periods, which promoted intense dissolution of the aragonitic bivalves (cf. Morse and Mackenzie 1990; Moore and Wade 2013), and the precipitation of calcite prismatic rims in interparticle and intraparticle pores (Fig. 3E). Pathway 2 was promoted probably where less dilute fluids initially allowed preservation of the bioclasts (cf. James and Choquette 1984; Caron and Nelson 2009), and precipitation of calcite prismatic rims and drusiform cement, followed by extensive dissolution of bioclasts and generation of moldic porosity (Fig. 4F). Pathway 3 developed where limited circulation of fluids slightly supersaturated with respect to aragonite favored the precipitation of thin calcite rims, the neomorphism of the bioclasts (Fig. 3D), and the preservation of interparticle porosity. The common alternation of intervals with predominance of neomorphism and of dissolution indicates frequent oscillation between these interpreted environmental conditions. Such diagenetic variations may be related to climatic control of the composition and level of lacustrine waters, or to tectonically driven hydraulic gradients, probably related to faulting along the rift margins, generating patterns that cannot be correlated among the studied wells. This paragenetic evolution of the bioclastic rudstones and grainstones (Fig. 12) differs from that of equivalent rocks from the central and southern parts of the basin, where there is a predominance of aragonite neomorphism in relation to dissolution (Bertani and Carozzi 1985b; Altenhofen 2013; Muniz 2014; Goldberg et al. 2017).

Typical vadose features, such as pendant or meniscus cements (cf. James and Choquette 1984), infiltration of clay and/or silt, and development of soils and calcretes were not observed in the bioclastic rocks, indicating that exposure was not significant in the succession. The locally observed displacive silica cementation of bioclastic rocks was therefore not related to the formation of silcretes under subaerial arid conditions (Ross and Chiarenzelli 1985; Khalaf 1988; Hesse 1989; Murray 1990). Since the bioclastic deposits are poor in siliciclastic grains, such early silica precipitation was probably derived from dissolution of the stevensitic ooids.

Origin and Diagenesis of Stevensite

Recent studies indicate that Mg-clays are formed from Si-Mg hydrated gel precursors (Tosca and Wright 2014; Wright and Barnett 2015), which evolve to stevensite, kerolite, talc, and other Mg-clay mineral phases in highly alkaline lacustrine and palustrine environments (Rehim et al. 1986; Pozo and Casas 1999). Experimental studies show that this evolution depends on a number of environmental factors, including pH, salinity, temperature, and ionic content (Jones 1986; Tosca and Masterson 2014). The alkaline conditions needed for stevensite precipitation ($\text{pH} \geq 10$) were recurrent during the rift evolution, as stevensite arenites occur in different stages and areas of the Campos rift (Bertani and Carozzi 1985a, 1985b; Armelanti et al. 2016; Goldberg et al. 2017). These conditions were very different from the fresh-water environments colonized by bivalves and gastropods. The common mixture of stevensite ooids and peloids with bivalve bioclasts in the Campos Basin rift section indicates their extensive gravitational resedimentation in deeper lacustrine environments throughout the evolution of the rift (Goldberg et al. 2017).

Pozo and Casas (1999) suggested that gel coagulation would result in granular clay particles, which could explain the common peloidal habit of

stevensite. The habit of stevensite could be related to the energy of its depositional environment, as observed for glauconite, berthierine, and other syngenetic clay minerals (e.g., Van Houten and Purucker 1984; Odin 1988). As for these clays, the stevensitic ooids were probably formed in environments with some agitation by waves or currents, while the laminated stevensitic claystones were certainly deposited in low-energy environments. The peloids were probably formed in environments of an energy level between that for the formation of the ooids and that for the laminated claystones. According to Tosca and Wright (2015), the high sensitivity to $p\text{CO}_2$, pH, and the fast dissolution kinetics due to the high specific surface area favors the eogenetic dissolution of Mg-clays. The common dissolution and replacement of stevensite by silica and dolomite probably occurred mostly during eodiagenesis (Fig. 12), controlled by variations in the chemistry of the lacustrine waters. As observed in other rift lakes (e.g., Renaut et al. 1986; De Wet et al. 2002), dilution of lake waters during more humid periods, or input of CO_2 by magmatic and hydrothermal activity, may have promoted the dissolution of Mg-clays, liberating silica and magnesium, and favoring the precipitation of silica and dolomite. Further dissolution of stevensite ooids and peloids after cementation generated abundant moldic and intraparticle porosity (Fig. 5). Intense dissolution, silicification, and dolomitization are observed in stevensitic arenites just below the pre-Alagoas regional unconformity, suggesting alteration in a subaerial environment during post-rift uplift and exposure.

Genesis of Calcite Spherulites

The most abundant eogenetic constituent replacing stevensite are spherulites of calcite, which occur throughout the sag succession (Figs. 6A, 7A, B). The formation of spherulites has been interpreted to be favored in the interior of inorganic gels, although the viscous medium is not a prerequisite for spherulite growth (Beck and Andreassen 2010; Shtukenberg et al. 2012). Our petrographic evidence shows that the development of spherulites occurred inside the stevensite laminations or the hybrid siltstones, displacing and replacing the original unconsolidated sediment, suggesting early diagenetic conditions. Laboratory studies have reported that the development of calcite spherulites is favored in alkaline conditions with high concentrations of silica and magnesium (García-Ruiz 2000; Meister et al. 2011), which agrees with the interpreted alkaline lacustrine environment. Most of the spherulites show no visible nuclei, and some display stevensite peloids, siliciclastic grains, and ostracod bioclasts as nuclei. Natural and synthetic spherulites interpreted as formed by direct microbial activity (Braissant et al. 2003; Spadafora et al. 2010) have sub-micrometric dimensions, differing significantly from those found in the pre-salt rocks.

Formation and Evolution of Fascicular Calcite Crusts

Fascicular calcite crusts are interpreted as syngenetic or synsedimentary precipitates, encrusting many different deposits. The absence of clotted and cryptocrystalline textures, as well as of irregular branching structures, characteristic of the mineralization of benthic microbial communities (cf. Burne and Moore 1987; Riding 2000), and the continuous fibrous crystal fabric of the fascicular crusts, indicate that they are not microbialites (*sensu* Burne and Moore 1987), but rather a product of abiotic precipitation. A chemical, abiotic precipitation has been interpreted for texturally equivalent deposits in travertines (cf. Chafetz and Guidry 1999; Fouke 2011), stromatolites (cf. Grotzinger and Knoll 1995; 1999; Riding 2008; Pope et al. 2000), alkaline-saline lakes (cf. Jones and Renaut 1994; Warren 2006), and, more recently, for the pre-salt reservoirs themselves (Wright and Barnett 2015). Additionally, the absence of luminescence of the fascicular calcite suggests a low content of organic matter inclusions in the aggregates. The fascicular calcite aggregates precipitated not only

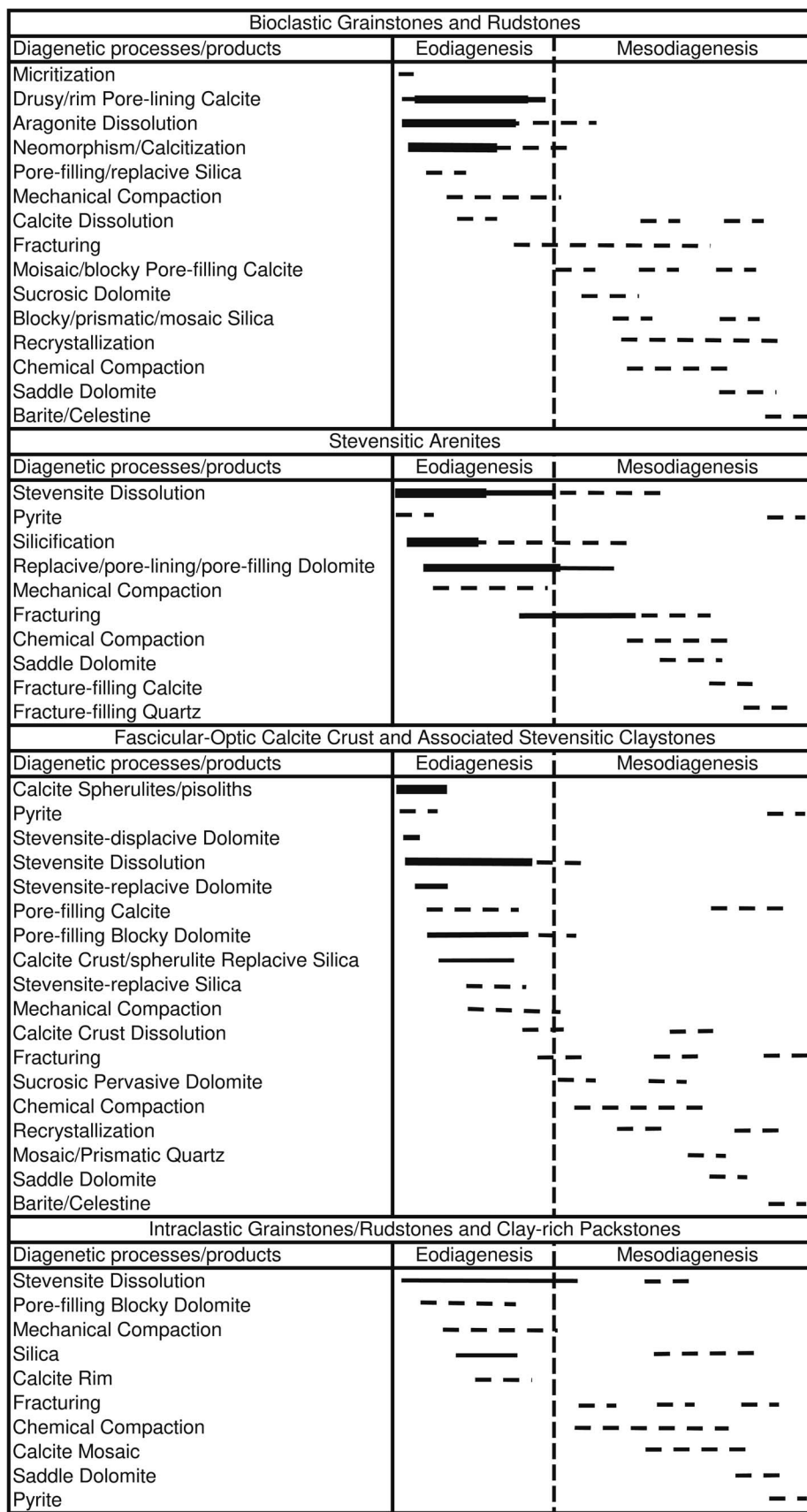


FIG. 12.—Diagenetic sequences interpreted for the studied rock types. Thicker lines correspond to more significant processes and products, whilst dashed lines correspond to less intense processes and products.

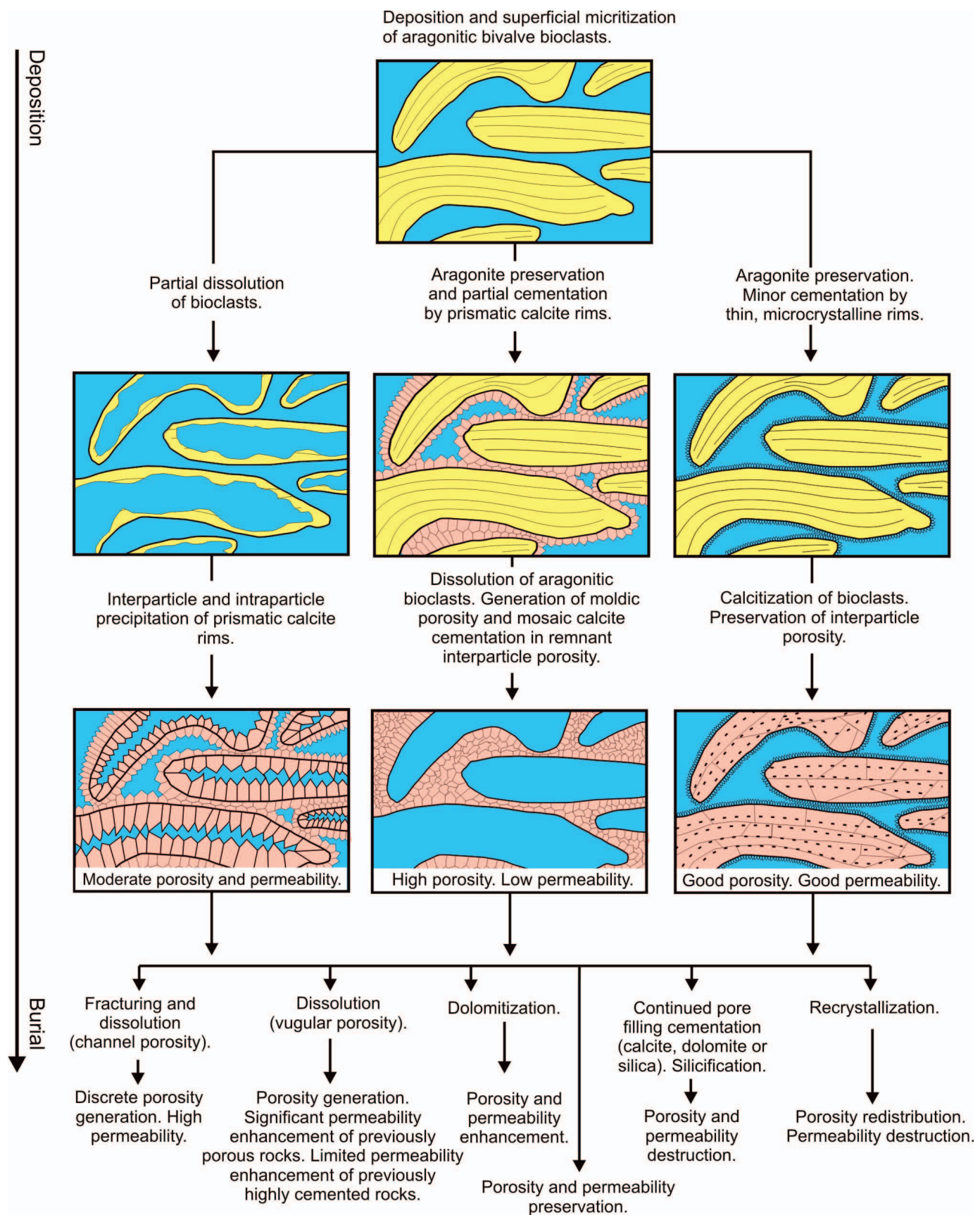


FIG. 13.—Schematic diagenetic pathways of bioclastic rudstones and grainstones, showing the impact of diagenetic process and products on porosity preservation, enhancement, and destruction and their resulting impact on permeability.

encrusting diverse sediments, particularly the background stevensitic deposits, but also partially replacing them. This is indicated by the common occurrence of clay laminations, peloids, and other particles in the interstitial spaces, and as inclusions in the aggregates. The truncation of clay laminations by fascicular calcite aggregates is common, indicating that they grew as early diagenetic replacement. The combined evidence indicates that the precipitation of syngenetic calcite crusts and of stevensite was chemically controlled by the dynamic evolution of the lacustrine environmental conditions. Stevensite precipitated under high concentrations of silica and magnesium and low $p\text{CO}_2$, while calcite precipitation was favored by less concentrated fluids related to less arid periods, and/or by degassing after $p\text{CO}_2$ input from magmatic and/or hydrothermal activity.

The paragenetic relationships of calcite crusts with stevensite and the main evolution pathways are illustrated in Figure 14. Where calcite precipitation predominated, the development of coalesced fascicular shrubs formed interstitial growth-framework porosity, with variable amounts of trapped clastic and stevensitic particles. The dissolution of stevensite released magnesium and silica, which resulted in replacement of calcite shrubs by silica and dolomite cement partially or totally filling the growth-framework porosity. In other cases, the growth-framework pores were enlarged by dissolution of the fascicular aggregates. Where calcite precipitation was less extensive, discontinuous, non-coalesced calcite crusts were formed, intercalated laterally and vertically by stevensite. Stevensite deposits were heterogeneously replaced by calcite spherulites, and by dolomite. The dissolution of stevensite among spherulites locally generated porosity, but seldom reservoirs, as dolomite commonly cemented the secondary porosity generated by stevensite dissolution.

Diagenesis of the Intraclastic Grainstones and Rudstones

Two main patterns of eogenetic evolution, defined by the relationship between compaction and cementation, were recognized in the intraclastic grainstones and rudstones formed by fragmentation of the calcite crusts and reworking of spherulites and stevensitic particles (Fig. 15). (1) Rocks with limited eogenetic cementation were affected by mechanical and chemical compaction, followed by mesogenetic calcite cementation (Fig. 10C). (2) Partial, heterogeneous eogenetic cementation by calcite or dolomite promoted the preservation of interparticle primary porosity, inhibiting pressure dissolution. The porosity was heterogeneously enlarged by dissolution of the intraclasts (Fig. 10D). Some samples display abundant eogenetic precipitation of displacive silica, which filled the porosity and inhibited the mesogenetic processes. Clay-rich packstones formed by intraclasts and clay matrix (Fig. 10B) locally show early dissolution of the matrix, enabling a diagenetic evolution similar to that observed in the grainstones and rudstones (Fig. 15). Figure 12 shows the paragenesis of the intraclastic grainstones and rudstones.

Dolomite

Dolomite occurs very frequently in the studied pre-salt rocks, especially in the sag section, with various morphologies and timings. At least five major phases of dolomite precipitation were identified. Early dolomite grew inside unconsolidated stevensite laminae, visibly displacing the sediment (Fig. 6E). A microbial origin for these early dolomites is unlikely, since the mechanism of dolomite precipitation by sulfate-reducing bacteria proposed by McKenzie and Vasconcelos (2009) would not be effective in lacustrine environments with low sulfate, as evidenced by the absence of pyrite frambooids or of primary and/or eogenetic sulfates. The formation of early dolomite was probably directly related to the dissolution of stevensite, although it may have been favored also by the dehydration of magnesium complexes promoted by the carboxylated surfaces of the organic matter present in the stevensite (Roberts et al. 2013). A second type of dolomite

occurrence corresponds to a mimetic replacement of stevensite laminations (Fig. 7B), which is normally not associated with porosity generation. A third type of dolomite occurs as pore filling on sag deposits, cementing calcite crusts and intraclastic rocks. Pre-compaction dolomite cementation on intraclastic grainstones and rudstones suggests an early eogenetic origin for dolomite pore filling. A fourth pattern of dolomitization corresponds to the pervasive replacement of the rock (Fig. 4A), common in both the rift bioclastic rocks and in the deposits of the sag stage. This dolomitization pattern frequently occurs associated with silicification and fracturing, and with the generation of porosity, which may be related to circulation of hydrothermal fluids. The fifth type corresponds to the saddle dolomite (Fig. 11C), which occurs frequently associated with fracturing. Saddle dolomite is a common mesogenetic constituent in carbonate and clastic rocks (Spötl and Pitman 1998), and is not by itself indicative of hydrothermal alteration. However, its association with intense fracturing in some of the studied rocks suggests hydrothermal influence.

Hydrothermal and Mesogenetic Alterations

The term hydrothermal has been defined in different ways, generally to characterize changes related to hot-water circulation. Machel (2002) suggests that the term should be used only to identify minerals that are formed at temperatures higher than those of the host rocks, regardless of the origin and composition of the fluids. In this sense, the identification of hydrothermal alteration would require isotopic and fluid-inclusion analyses, or the presence of exotic mineralogy formed at high temperatures. The presence of saddle dolomite does not define hydrothermal alteration, since it can be formed at common burial temperatures and conditions, as previously discussed. However, there are occurrences in the studied succession that are characterized by intense fracturing, dissolution, silicification, dolomitization, as well as concentration of barite, fluorite, kaolinite or dickite, pyrite, and other sulfides. These alterations could be promoted by the focused circulation of deep-sourced fluids, which generated distinct hydrothermal alterations. Recently, Alvarenga et al. (2016) recognized multiple hydrothermal vents in the rift section of central Campos Basin. Although lacking sampling of the most affected intervals, areas with intense dissolution were interpreted in the well logs and formation tests as probably related to hypogenic hydrothermal karst (cf. Dublyansky 1995; Heward et al. 2000). Such areas may be extremely important for fluid flow and hydrocarbon production.

Mesogenetic dissolution has not created a significant volume of porosity in the studied reservoirs. Vuggy porosity occurs erratically along the studied reservoirs in several facies. These vugs are interpreted to have been formed during mesodiagenesis by dissolution of primary and eogenetic constituents, since typical eogenetic cements are not observed filling these pore types. Such dissolution may have been generated by acidic pore waters derived from the rift shales (Racey et al. 2001; Beavington-Penney et al. 2008). Although “exotic” minerals, such as epidotes, prehnite, amphiboles, and metallic sulfides, were not observed in channel and vugular porosity, the influence of hydrothermal fluids on mesogenetic dissolution at pore scale cannot be ruled out.

Celestine, barite, and anhydrite occasionally occur as late cements filling primary and secondary porosity and/or replacing primary and diagenetic constituents. As these minerals are commonly related to fractured intervals, their precipitation was probably connected with the circulation of deep fluids, although they could be locally influenced by the dissolution of overlying evaporites. The occurrence of aluminum phosphate-sulfate (APS) minerals is not indicative of any specific genetic environment, occurring in a wide diversity of geological settings, including sedimentary (carbonates and siliciclastics), igneous, and metamorphic rocks (Dill 2001). Traces of svanbergite–goyazite occur replacing mud intraclasts in the bioclastic reservoirs and are associated with silicification, dolomitization, and fracturing in other facies in sag deposits. Specific geochemical

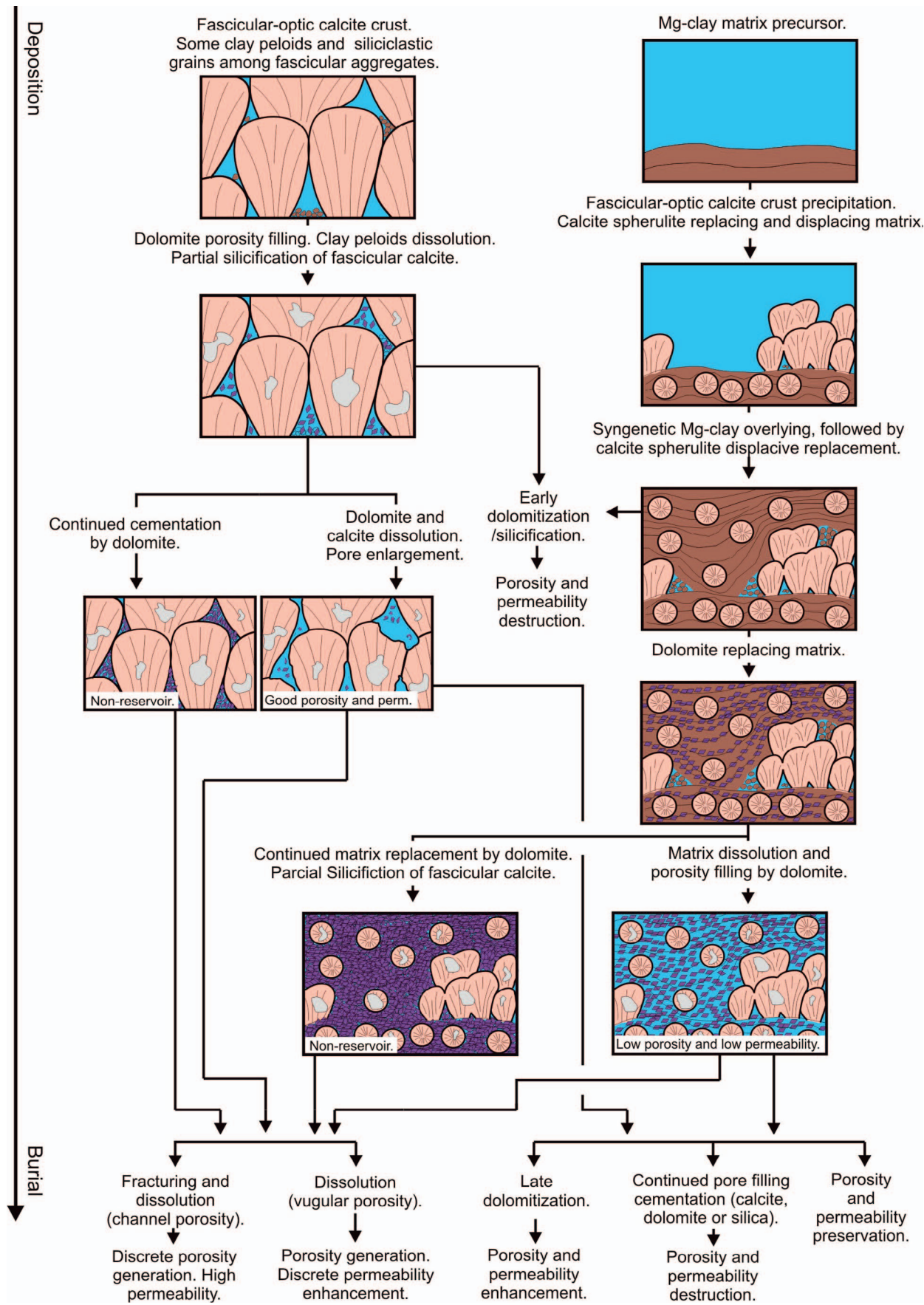


FIG. 14.—Schematic evolution of calcite crusts and their relationship with stevensite, showing the impact of diagenetic process and products on porosity preservation, enhancement, and destruction and their resulting impact on permeability.

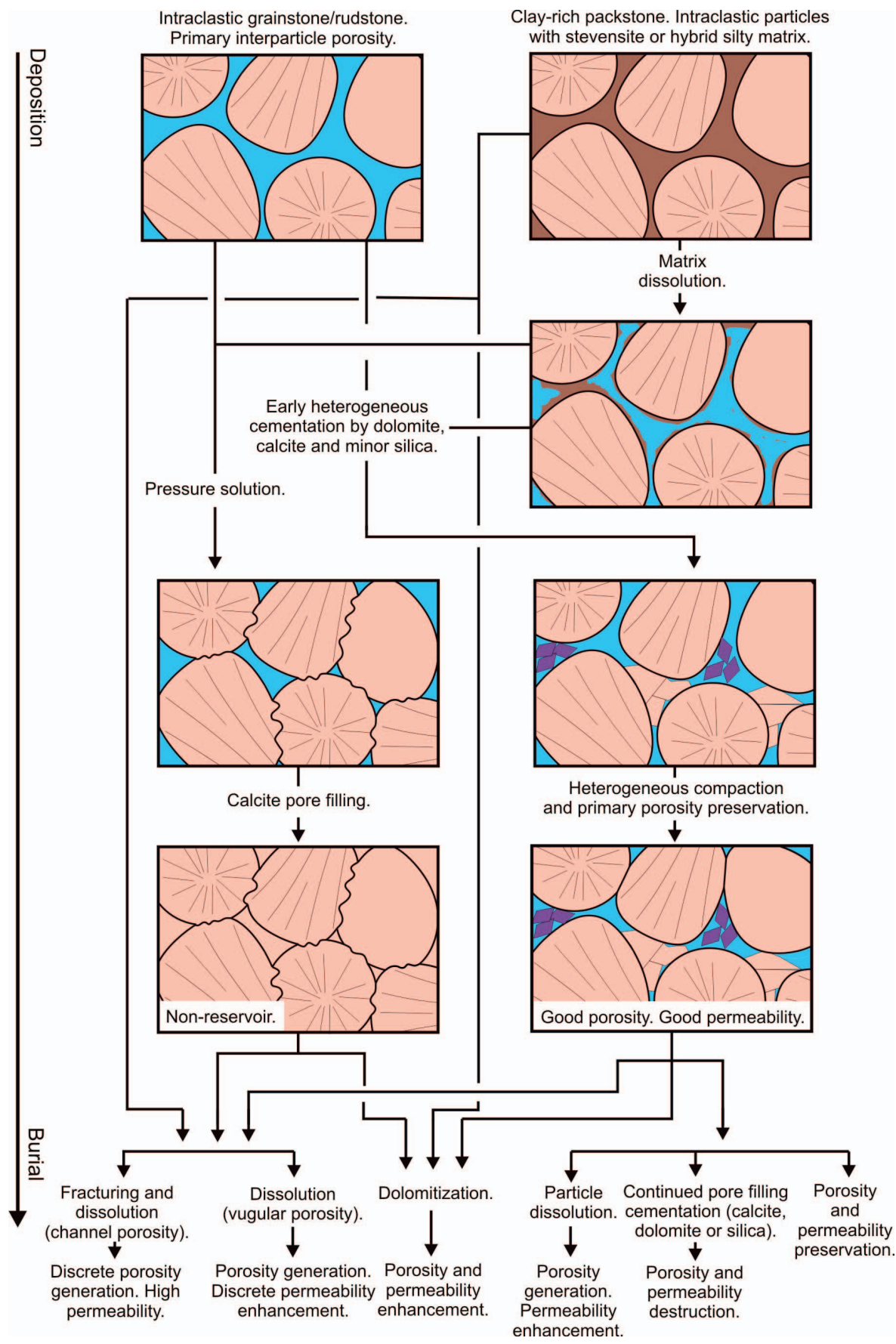


FIG. 15.—Schematic diagenetic evolution of intraclastic grainstone and rudstones, showing the impact of diagenetic process and products on porosity preservation, enhancement, and destruction and their resulting impact on permeability.

analyses are necessary for a better understanding of origin and timing of these minerals.

Porosity and Permeability of Reservoir Petrofacies

Reservoir petrofacies were defined for the studied lithologies, based on the main primary structures, textures, and constituents, major diagenetic processes and products, and patterns of relationship between these parameters with porosity and permeability.

Bivalve–Gastropod Rudstones with Interparticle Porosity.—Preservation of interparticle porosity occurred mostly where neomorphism predominated over dissolution (Figs. 3D, 4D). This petrofacies has the best permeability among the bioclastic reservoirs, even considering samples with lower porosity (Fig. 16A, Table 1). Partially preserved primary porosity, mildly reduced by mechanical compaction and minor cementation, is connected by large pore throats. MICP analyses indicate that the pore throats are significantly larger than in other petrofacies (Fig. 17A). In some cases, however, continued cementation has narrowed the pore throats, decreasing permeability. Subordinate moldic pores increased the porosity, but with little effect on permeability. Nevertheless, the local development of vugular pores has enlarged the primary pores, enhancing permeability.

Bivalve–Gastropod Rudstones with Moldic Porosity.—Bioclastic rocks with predominantly moldic or intraparticle porosity, combined with some interparticle porosity, are common. These rocks have good porosity but low permeability (Table 1, Fig. 16A). The cementation of the moldic and intraparticle pores is common, occasionally totally occluding the secondary porosity. The remaining interparticle pores contribute to the permeability, but because pore throats are controlled by microcrystalline and intercrystalline pores (Fig. 17A), permeabilities are generally low. Locally, vugular porosity was formed by enlargement and connection of molds, increasing pore throats and generating fair permeability conditions.

Bivalve–Gastropod Rudstones with Vugular Porosity.—Vugular porosity is often scarce in the studied rocks (Fig. 4E). Where vugs are the predominant pore type, porosities and permeabilities are generally low (Table 1, Fig. 16A), due to the low connectivity of the pore system. The presence of remnants of interparticle porosity contributes to some permeability, though generally low. However, because core samples with high vugular porosity were poorly recovered, and not suitable for petrophysical analyses, it is possible that the amount of vugular porosity was underestimated in the reservoirs due to these sampling limitations.

Bivalve–Gastropod Grainstones with Moldic Porosity.—These grainstones have a high content of moldic porosity, and a total porosity higher than all the bioclastic petrofacies (Table 1, Fig. 16A). These rocks generally present remaining interparticle porosity, which gives them some permeability. Vugular porosity was generated from enlargement of moldic porosity, producing widened pore throats, which increases permeability. The grainstones often present recrystallization, which has generated intercrystalline porosity, but with narrow pore throats (Fig. 17B) and low permeability.

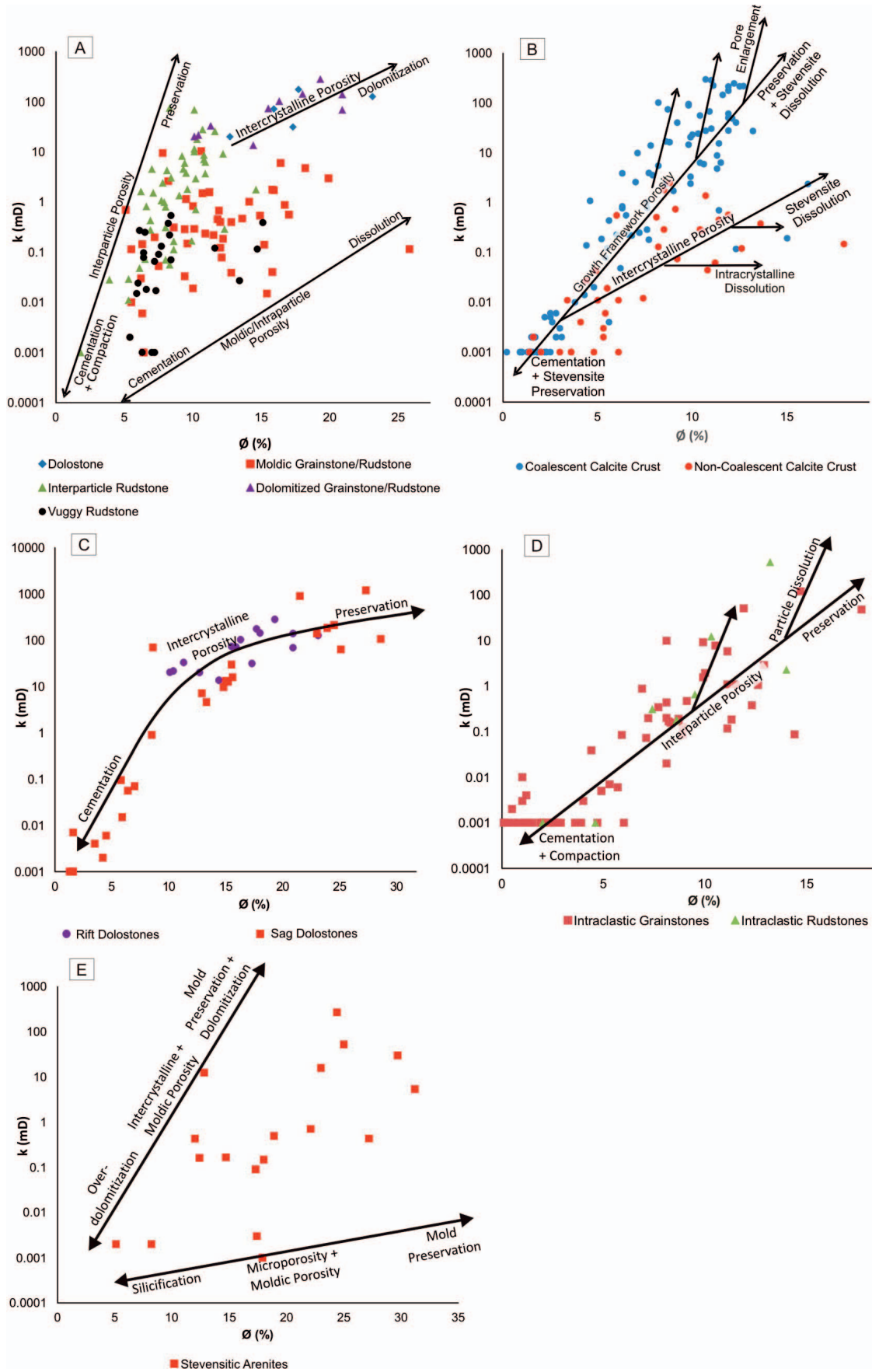
Stevensitic Arenites.—The high instability of Mg-clays (cf. Tosca and Wright 2014) has favored the dissolution of ooids and the precipitation of silica and dolomite (Fig. 5), redistributing the original porosity. The pore system of stevensitic arenites is extremely heterogeneous, generally presenting high porosities and highly variable permeabilities (Table 1, Fig. 16E). The dissolution of ooids, resulting in moldic and intraparticle porosity, was important, generating a significant increase in porosity. Microporosity in authigenic silica is observed. Remnants of primary

interparticle porosity are occasionally preserved, although the original interstitial porosity of most of the samples was completely filled by dolomite and quartz. Dolomitization has generated abundant intercrystalline porosity, occasionally connecting moldic and intracrystalline pores, and supplying permeability to the stevensitic arenites.

Coalescent Calcite Crusts.—Coalescent calcite crusts are composed of well-developed shrubs of fascicular calcite aggregates, which coalesced vertically and/or horizontally (Fig. 8A). The growth of these precipitates generated a growth-framework primary pore system with moderate porosity and good permeability, controlled by large pore throats (Table 1, Fig. 16B). Rezende and Pope (2015) properly related aspects of the depositional texture, including shrub size, sorting, and packing, to the porosity and permeability of analogous calcite crust reservoirs from the Santos Basin. According to those authors, the size of individual shrubs exerts a primary control on pore size, affecting both porosity and permeability. Although depositional texture probably exerted a major control on the primary petrophysical properties of the crusts, their primary fabric was strongly modified during diagenesis by cementation and/or dissolution. The dissolution of stevensite laminae or peloids filling interstices among the fascicular aggregates or in adjacent layers favored the precipitation of dolomite partially or totally cementing the interstitial porosity, which represented the main reducer of primary porosity. Commonly, coalescent crusts present porosity enhancement through partial dissolution of shrubs and cements (Fig. 8A), which has increased their porosity and has led to an enlargement of pore throats, with a consequent increase of permeability (Fig. 17D). Intra-crystalline porosity related to dissolution of dolomite crystals (Fig. 9B, C) or shrubs is very common. Porosity is present even in rocks without petrographic porosity, due to intra-crystalline porosity generated from dissolution of shrubs, as observed in SEM analyses (Fig. 9E).

Non-Coalescent Calcite Crusts.—Poorly developed calcite crusts with non-coalescent shrubs of fascicular calcite display interstices occupied by stevensite laminae and peloids, or even by siliciclastic matrix, resulting in limited growth-framework primary porosity (Fig. 14). Consequently, these rocks show low primary porosity and permeability. Commonly, associated stevensite laminae and peloids were partially replaced mainly by calcite spherulites and dolomite crystals. Later dissolution has generated intercrystalline porosity (Fig. 7E). The dominance of discontinuous intercrystalline porosity plus minor growth-framework porosity has generated poor reservoirs with mostly narrow pore throats (Figs. 16B, 17E). Most non-coalescent crusts have low porosity and permeability. Even though these reservoirs present poor quality (Table 2), they can store oil and probably contribute to the production of the wells.

Intraclastic Grainstones and Rudstones.—Few intraclastic rocks exhibit good reservoir quality, owing to partially preserved primary porosity, representing good quality reservoirs (Table 2, Fig. 16D). At least part of the intraclastic grainstones and rudstones composed of reworked calcite crusts and spherulites had good primary interparticle porosity, which was destroyed by compaction and cementation (Fig. 10C). Heterogeneous cementation preserved part of the primary porosity, which was enhanced by particle dissolution, while the porosity of uncemented rocks was completely obliterated during mesodiagenesis by interparticle pressure dissolution and calcite cementation (Fig. 15). No clear particle size control is observed on porosity and permeability, suggesting that diagenesis is the major control. Secondary intraparticle porosity in partly dissolved intraclasts is occasionally seen in rocks with some preserved interparticle porosity (Fig. 10D). When moldic or vugular porosity occur associated with interparticle porosity, permeability is higher, generating the best reservoir conditions among the intraclastic rocks.



←

Fig. 16.—Correlation between porosity and permeability, showing the interpreted effect of diagenesis on pore type and permeability in studied reservoir petrofacies: **A**) pore type of bioclastic bivalve–gastropod rudstones and grainstones ranges between totally moldic to interparticle. The interpretive axis “Interparticle Porosity” represents 100% of interparticle pores, which may be preserved or reduced by compaction and cementation. The other extreme axis would represent 100% moldic porosity, which increases by dissolution of bioclasts or decreases by cementation of molds. In addition, intercrystalline porosity often generated by dolomitization increases both total porosity and permeability. Samples show the association of more than one type of pore, ranging between the interpreted axes. **B**) Coalescent calcite crusts have primary growth-framework porosity that can be reduced by cementation, or preserved and increased by pore enlargement. Alternatively, the interstices may have been early filled by stevensite, which may have been preserved or dissolved. Porosity of non-coalescent crusts is related to the dissolution of stevensite, generating intercrystalline porosity among dolomite crystals and spherulites. Abundant intracrystalline dissolution is observed within calcite crusts and dolomite cements, which generates some porosity with minor effect on permeability. **C**) Dolostones have a well-defined trend of porosity and permeability controlled by the amount of intercrystalline porosity. **D**) Intraclastic rudstones and grainstones are intensely affected by compaction and cementation. Partial preservation of interparticle porosity promotes preservation of permeability; both porosity and permeability may be increased by particle dissolution. **E**) Stevensitic arenites pore types range between moldic + microcrystalline porosity related to silicification (low permeability), and moldic + intercrystalline porosity related to dolomitization (high permeability).

Clay-Rich Packstones.—Intraclastic rocks with clay matrix are usually not reservoirs. In some cases, however, early dissolution of matrix occurred, leaving residual dolomite and/or silica. Some of such petrofacies evolved similarly to grainstones, with secondary porosity partially preserved by heterogeneous cementation (Fig. 15). Another possibility for the occurrence of secondary porosity in clay-rich packstones is through early heterogeneous dolomitization or silicification, followed by dissolution.

Dolostones.—Dolomitization is a very important process, generating rocks with the best porosity and permeability of the studied reservoirs (Table 1, Fig. 16C). In many cases, sucrosic dolomitization has added intercrystalline porosity, leaving relicts of primary interparticle or moldic and/or vugular secondary porosity. Dolomitized rudstones with moldic and/or vugular porosity have developed higher porosities and permeabilities after dolomitization through the connection of vugs and molds by intercrystalline porosity, which have controlled pore throat diameters (Fig. 17C). However, the vugular porosity can be directly related to dolomitization processes. Late processes were limited to the precipitation of minor amounts of saddle dolomite, preserving most of the intercrystalline porosity generated during dolomitization. The frequent total dolomitization of sag rocks generated significant decrease of pore throat size (Fig. 17F). Apparently, early dolomitization caused severe porosity reduction, while dolomitization associated with fracturing has generated higher porosities and permeabilities.

Implications for Exploration of Lacustrine Carbonates

The absence of features characteristic of vadose diagenesis (i.e., pendular or meniscus cements, geopetal features, etc.) and of exposure surfaces in massive bioclastic reservoirs about 100 meters thick, suggests that they were accumulated in relatively deep lacustrine environments. The extensive resedimentation of the bioclastic deposits by gravitational mass movements was probably triggered by tectonism, as also observed in the central area of the basin (Goldberg et al. 2017). These factors allowed the accumulation of thick bioclastic deposits, which were probably remobilized from shoreface and related shallow-water environments. The limited fragmentation and abrasion of bivalve shells suggests little reworking and short residence time in moderate energy shallow environments before redeposition. The good preservation of the bioclasts contributes to the common occurrence of reservoirs with good permeability owing to large pores connected by wide pore throats. Redeposition to deep lacustrine settings allowed impressive accumulation of the bioclastic deposits and inhibited extensive dissolution of the bioclasts and interparticle cementation. Thus, bioclastic deposits redeposited in relatively deep lacustrine settings may constitute attractive exploratory targets in other areas of the Campos Basin, and in other rift basins with similar geologic context.

The crusts of fascicular-optic calcite present significant similarity with crystalline shrub facies and pore types of travertines (Chafetz and Guidry

1999; Claes et al. 2017). Travertines, however, exhibit steep facies diversity and distribution restricted to the immediate proximity of their source springs. These features are not observed in the pre-salt calcite crusts, indicating that these carbonates were precipitated in subaqueous environments. Continuous subsidence during the sag stage with a constant supply of magnesium, calcium, and silica allowed the accumulation of more than 200 meters of precipitated carbonates and clays, which allowed the development of reservoirs with impressive thicknesses. The geometry of the fascicular calcite crusts inhibited the compaction of the reservoirs, preserving good permeability associated with large pores and wide pore throats. The dissolution of stevensite after the precipitation of spherulites and dolomite developed significant secondary porosity in originally argillaceous deposits (Tosca and Wright 2015). The distribution of calcite, stevensite, and porosity in the sag section follows complex patterns, which were fundamentally controlled not by lacustrine base level but by the chemistry of the lake waters (Wright and Barnett 2015). These observations have significant implications for the construction of predictive and conceptual models for the exploration of the sag pre-salt reservoirs in the Campos and Santos basins, and for planning the development and optimizing oil recovery from the producing oilfields.

CONCLUSIONS

1. A study integrating systematic petrographic characterization and petrophysical analysis reveals that the pre-salt lacustrine reservoirs of northern Campos Basin have complex pore systems, which result in highly heterogeneous permeability patterns. The primary composition and porosity have a strong influence on the evolution quality of the reservoirs.
2. The compositional and porosity evolution of the bioclastic rudstone and grainstone rift reservoirs is controlled by the balance between dissolution and neomorphism of the aragonitic bivalves and gastropods. When the circulation and geochemistry of eogenetic interstitial fluids favored the dissolution of aragonite and precipitation of low magnesium calcite, moldic porosity was generated and primary interparticle porosity was reduced, resulting in low permeability. The predominance of neomorphism over dissolution resulted in higher permeability due to the preservation of primary interparticle porosity.
3. The redeposition of the bioclasts into relatively deep lacustrine settings is a crucial factor for the accumulation of thick deposits with partially preserved interparticle porosity, which constitute good quality reservoirs.
4. Sag stage stevensitic deposits were replaced mainly by calcite spherulites and dolomite. These rocks locally constitute reservoirs, where secondary porosity was generated by stevensite dissolution. Dissolution of stevensite provided magnesium and silica, favoring the dolomitization and silicification commonly observed in the studied succession.

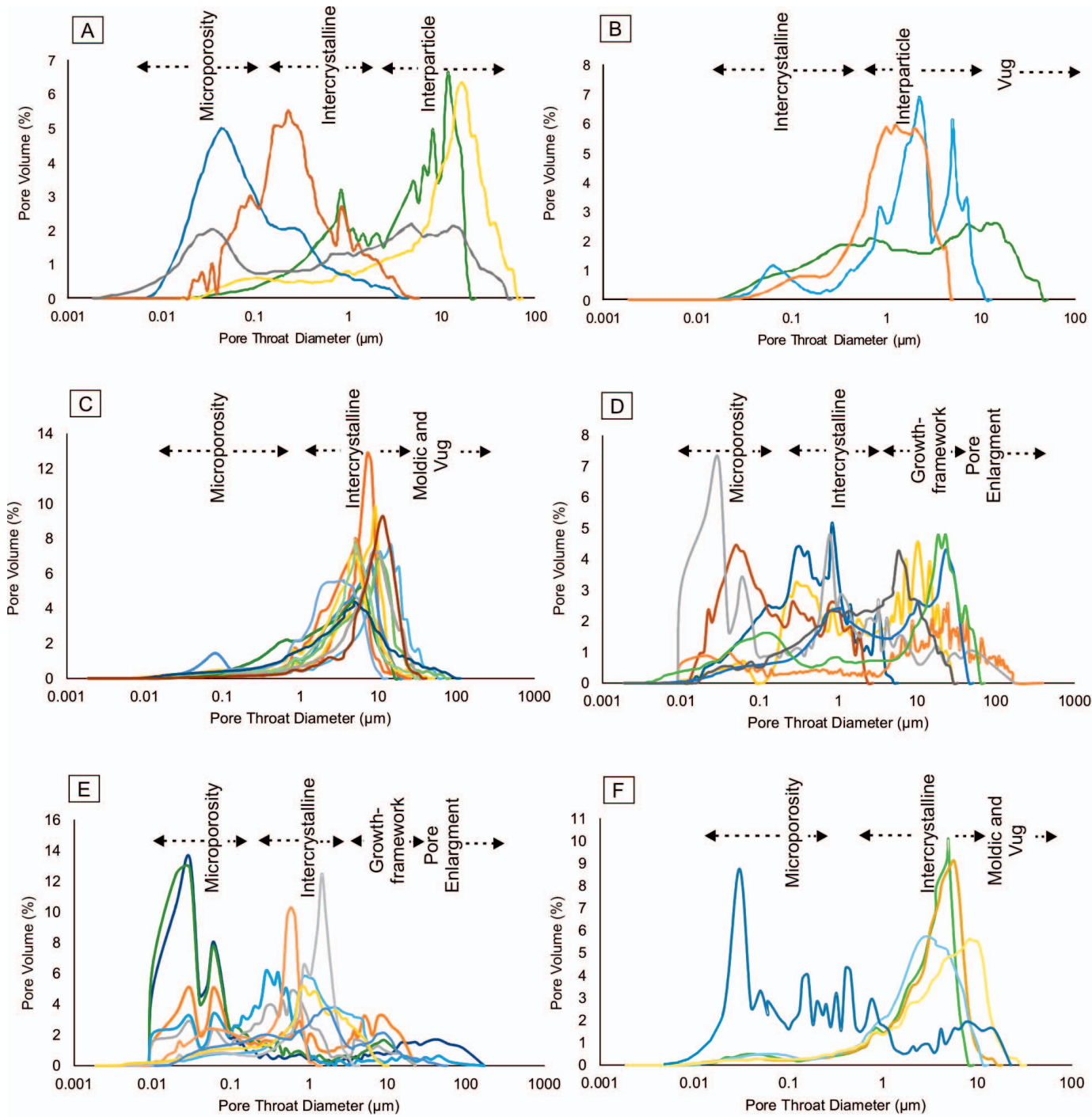


FIG. 17.—Distribution of pore throats of studied samples and their interpreted relationship with the pore type (each color represents one sample): A) bioclastic rudstones. B) Bioclastic grainstones. C) Dolostones from the rift section. D) Coalescent calcite crust. E) Non-coalescent calcite crust. F) Dolostones from the sag section.

5. Abiotic, fascicular-optic calcite crusts with growth-framework primary porosity, or interstitial porosity generated by the dissolution of stevensite, constitute the main sag phase reservoirs. The patterns of preservation, dissolution, and replacement of stevensite exerted an important control on the quality of these reservoirs. Petrographic evidence indicates that most of the mineralogical and porosity evolution of these rocks occurred during eodiagenesis, mainly in response to the high reactivity of the stevensite.
6. Syngenetic sag precipitates were controlled by the geochemistry of lacustrine waters through changes on pH, Mg and Ca activities, temperature, and $p\text{CO}_2$, promoting the alternation of periods of calcite or stevensite precipitation. The syngenetic precipitation of fascicular calcite crusts took place mostly covering stevensitic deposits, although in some cases they clearly replaced stevensite, suggesting that at least part of the fascicular calcite is diagenetic.

TABLE 2.—Statistical summary of MICP analysis showing pore throat radius and pore classification of petrofacies.

Petrofacies	Median Pore Throat (μm)	Average Pore Throat (μm)	Microporosity (%)	Mesoporosity (%)	Macroporosity (%)	n
Bioclastic Rudstones	3.77	4.90	47.12	28.66	24.22	5
Bioclastic Grainstones	2.33	3.25	20.85	60.65	18.50	3
Stevensitic Arenites	2.87	6.02	29.05	28.50	42.45	2
Coalescent Calcite Crust	4.31	7.77	37.50	31.00	31.50	8
Non-Coalescent Calcite Crust	0.64	1.96	50.94	40.49	8.57	10
Dolostones	4.27	5.59	13.67	45.17	41.16	20
Average	3.03	4.92	33.19	39.08	27.73	48

- Intraclastic rocks composed of intraclasts of calcite crusts and spherulites containing minor amounts of stevensite ooids and peloids or matrix may constitute good reservoirs when the interparticle porosity is preserved and/or the clays are dissolved.
- Stevensitic arenites were strongly affected by meteoric dissolution and replacement by dolomite and silica, related to regional uplift and erosion after the rift phase. The resulting rocks, composed almost exclusively by silica and/or dolomite, have a complex porous system, with moldic, microcrystalline, and intergranular porosity, and highly heterogeneous permeability patterns.
- Dolomitization is an important process of porosity modification of both rift and sag deposits, showing a great diversity of origins and fabrics. Early dolomitization, related mainly to stevensite dissolution and replacement, has usually not enhanced reservoir quality. However, dolomitization related to late fracturing and silicification has locally developed reservoirs with high porosity and permeability.

ACKNOWLEDGMENTS

The authors would like to thank to PETROBRAS S.A. for access to samples, well logs, and petrophysical analysis, and for permission to publish this work. We gratefully acknowledge reviewers Sadoon Morad and Noel P. James, Associate Editor Stacy Lynn Reeder, and Editor Leslie Melim for helping to improve this paper.

REFERENCES

- ABRAHÃO, D., AND WARME, J., 1990, Lacustrine and associated deposits in a rifted continental margin: Lower Cretaceous Lagoa Feia Formation, Campos Basin, Offshore Brazil, in Katz, B.J., ed., Lacustrine Basin Exploration: Case Studies and Modern Analogs: American Association of Petroleum Geologists, Memoir 50, p. 287–305.
- AHR, W.M., 2008, Geology of Carbonate Reservoirs: The Identification, Description, and Characterization of Hydrocarbon Reservoirs in Carbonate Rocks: Hoboken, John Wiley & Sons, 296 p.
- ALTENHOFEN, S.D., 2013, Caracterização petrográfica de depósitos carbonáticos lacustres do Grupo Lagoa Feia, Bacia de Campos, Brasil [Bsc Thesis]: Universidade Federal do Rio Grande do Sul, 69 p.
- ALVARENGA, R.S., IACOPINI, D., KUCHLE, J., SCHERER, C., AND GOLDBERG, K., 2016, Seismic characteristics and distribution of hydrothermal vent complexes in the Cretaceous offshore rift section of the Campos Basin, offshore Brazil: Marine and Petroleum Geology, v. 74, p. 12–25.
- ARMELENTI, G., GOLDBERG, K., KUCHLE, J., AND DE ROS, L.F., 2016, Deposition, diagenesis and reservoir potential of non-carbonate sedimentary rocks from the Rift Section of Campos Basin, Brazil: Petroleum Geoscience, v. 22, p. 223–239.
- ASLANIAN, D., MOULIN, M., OLIVET, J., UNTERNEHR, P., MATIAS, L., BACHE, F., RABINEAU, M., NOUZÉ, H., KLINGELHEOFER, F., CONTRUCCI, I., AND LABAILS, C., 2009, Brazilian and African passive margins of the Central Segment of the South Atlantic Ocean: Kinematic constraints: Tectonophysics, v. 468, p. 98–112.
- AUSTIN, J.A., AND UCHUPI, E., 1982, Continental-oceanic crustal transition off southwest Africa: American Association of Petroleum Geologists, Bulletin, v. 66, p. 1328–1347.
- BASAN, P.B., LOWDEN, B.D., WHATTIER, P.R., AND ATTARD, J.J., 1997, Pore-size data in petrophysics: perspective on the measurement of pore geometry, in Lovell, M.A., and Harvey, P.K., eds., Developments in Petrophysics: Geological Society of London, Special Publication 122, p. 47–67.
- BEAVINGTON-PENNEY, S.J., NADIN, P., WRIGHT, V.P., CLARKE, E., MCQUILKEN, J., AND BAILEY, H.W., 2008, Reservoir quality variation on an Eocene carbonate ramp, El Garia Formation, offshore Tunisia: structural control of burial corrosion and dolomitisation: Sedimentary Geology, v. 209, p. 42–57.
- BECK, R., AND ANDREASSEN, J., 2010, Spherulitic growth of calcium carbonate: Crystal Growth & Design, v. 10, p. 2934–2947.
- BERTANI, R., AND CAROZZI, A., 1985a, Lagoa Feia Formation (Lower Cretaceous), Campos Basin, Offshore Brazil: rift valley stage lacustrine carbonate reservoirs, I: Journal of Petroleum Geology, v. 8, p. 37–58.
- BERTANI, R., AND CAROZZI, A., 1985b, Lagoa Feia Formation (Lower Cretaceous) Campos Basin, Offshore Brazil: rift valley type lacustrine carbonate reservoirs, II: Journal of Petroleum Geology, v. 8, p. 199–220.
- BRAISSAT, O., CAILLEAU, G., DUPRAZ, C., AND VERRECCHIA, E.P., 2003, Bacterially induced mineralization of calcium carbonate in terrestrial environments: the role of exopolysaccharides and amino acids: Journal of Sedimentary Research, v. 73, p. 485–490.
- BRIGAUD, B., VINCENT, B., DURLET, C., DECONINCK, J., JOBARD, E., PICKARD, N., YVEN, B., AND LANDREIN, P., 2014, Characterization and origin of permeability–porosity heterogeneity in shallow-marine carbonates: from core scale to 3D reservoir dimension (Middle Jurassic, Paris Basin, France): Marine and Petroleum Geology, v. 57, p. 631–651.
- BURNE, R.V., AND MOORE, L.S., 1987, Microbialites: organosedimentary deposits of benthic microbial communities: Palaios, v. 2, p. 255–262.
- CAINELLI, C., AND MOHRIAK, W.U., 1999, Some remarks on the evolution of sedimentary basins along the Eastern Brazilian continental margin: Episodes, v. 22, p. 206–216.
- CALVO, J.P., BLANC-VALLERON, M.M., RODRIGUEZ-ARANDÍA, J.P., ROUCHY, J.M., AND SANZ, M.E., 1999, Authigenic clay minerals in continental evaporitic environments, in Thiry, M., and Simon-Coinçon, R., eds., Palaeoweathering, Palaeosurfaces and Related Continental Deposits: International Association of Sedimentologists, Special Publication 27, p. 129–151.
- CARMINATTI, M., DIAS, J.L., AND WOLFF, B., 2009, From turbidites to carbonates: breaking paradigms in deep waters: Houston, Texas, Offshore Technology Conference, 4–7 May, OTC 20124.
- CARON, V., AND NELSON, C.S., 2009, Diversity of neomorphic fabrics in New Zealand Plio-Pleistocene cool-water limestones: insights into aragonite alteration pathways and controls: Journal of Sedimentary Research, v. 79, p. 226–246.
- CARVALHO, M.D., PRAÇA, U.M., SILVA-TELLES, A.C., JAHNERT, R.J., AND DIAS, L.D., 2000, Bioclastic carbonate lacustrine facies models in the Campos Basin (Lower Cretaceous), Brazil, in Gierlowski-Kordesch, E., and Kelts, K.R., eds., Lake Basins through Space and Time: American Association of Petroleum Geologists, Studies in Geology 46, p. 245–255.
- CASANOVA, J., 1986, East African Rift stromatolites, in Frostick, L., ed., Sedimentation in the African Rift: Geological Society of London, Special Publication 25, p. 201–210.
- CASTRO, J.C., AZAMBUA FILHO, N.C., AND XAVIER, A.A.P.G., 1981, Fácies e análise estratigráfica da Formação Lagoa Feia, Cretáceo Inferior da Bacia de Campos, in VIII Congresso Geológico Argentino, Proceedings, p. 567–576.
- CHAFETZ, H.S., 2013, Porosity in bacterially induced carbonates: focus on micropores: American Association of Petroleum Geologists, Bulletin, v. 97, p. 2103–2111.
- CHAFETZ, H.S., AND GUIDRY, S.A., 1999, Bacterial shrubs, crystal shrubs, and ray-crystal shrubs: bacterial vs. abiotic precipitation: Sedimentary Geology, v. 126, p. 57–74.
- CHANG, H.K., KOWSMANN, R.O., AND FIGUEIREDO, A.M.F., 1988, New concepts on the development of east Brazilian marginal basins: Episodes, v. 2, p. 194–202.
- CHANG, H.K., KOWSMANN, R.O., FIGUEIREDO, A.M.F., AND BENDER, A., 1992, Tectonics and stratigraphy of the East Brazil Rift system: an overview: Tectonophysics, v. 213, p. 97–138.
- CHOQUETTE, P.W., AND PRAY, L.C., 1970, Geologic nomenclature and classification of porosity in sedimentary carbonates: American Association of Petroleum Geologists, Bulletin, v. 54, p. 207–250.
- CLAES, H., ERTHAL, M.M., SOETE, J., ÖZKUL, M., AND SWENNEN, R., 2017, Shrub and pore type classification: petrography of travertine shrubs from the Ballıklı–Belevi area (Denizli, SW Turkey): Quaternary International, v. 437, p. 147–163.
- CLEMSON, J., CARTWRIGHT, J., AND BOOTH, J., 1997, Structural segmentation and the influence of basement structure on the Namibian passive margin: Geological of London Society, Journal, v. 154, p. 477–482.
- DAVIS, R.L., AND WILKINSON, B.H., 1983, Sedimentology and petrology of freshwater lacustrine carbonate: mid-Tertiary Camp Davis Formation, northwestern Wyoming: University of Wyoming, Contributions to Geology, v. 22, p. 45–55.

- DE WET, C.B., MORA, C.I., GORE, P.J.W., GIERLowski-KORDESCH, E.H., AND CUCOLO, S.J., 2002, Deposition and geochemistry of lacustrine and spring carbonates in Mesozoic rift basins, eastern North America, in Renaut, R., and Ashley, G., eds., *Sedimentation in Continental Rifts: Society for Sedimentary Geology, Special Publication 73*, p. 309–325.
- DIAS, J.L., 2005, Tectônica, estratigrafia e sedimentação no Andar Aptiano da margem leste brasileira: Boletim de Geociências da Petrobras, v. 13, p. 7–25.
- DIAS, J.L., OLIVEIRA, J., AND VIEIRA, J., 1988, Sedimentological and stratigraphic analysis of the Lagoa Feia Formation, rift phase of Campos basin, offshore Brazil: *Revista Brasileira de Geociências*, v. 18, p. 252–260.
- DICKSON, J.A.D., 1965, A modified staining technique for carbonates in thin section: *Nature*, v. 205, p. 587.
- DILL, H.G., 2001, The geology of aluminum phosphate and sulphates of the alunite group minerals: a review: *Earth-Science Reviews*, v. 53, p. 35–93.
- DUBLYANSKY, Y.V., 1995, Speleogenetic history of the Hungarian hydrothermal karst: *Environmental Geology*, v. 25, p. 24–35.
- DUNAGAN, S.P., AND TURNER, C.E., 2004, Regional paleohydrologic and paleoclimatic settings of wetland/lacustrine depositional systems in the Morrison Formation (Upper Jurassic), Western Interior, USA: *Sedimentary Geology*, v. 167, p. 269–296.
- DÜRRSTADT, H., AND SIEGESMUND, S., 1999, Correlation between rock fabrics and physical properties of carbonate reservoir rocks: *International Journal of Earth Sciences*, v. 88, p. 392–408.
- EHRENBERG, S.N., EBERLI, G.P., KERAMATI, M., AND MOALLEMI, S.A., 2006, Porosity–permeability relationships in interlayered limestone–dolostone reservoirs: *American Association of Petroleum Geologists, Bulletin*, v. 90, p. 91–114.
- EHRENBERG, S.N., WALDERHAUG, O., AND BJORLYKKE, K., 2012, Carbonate porosity creation by mesogenetic dissolution: reality or illusion? *American Association of Petroleum Geologists, Bulletin*, v. 96, p. 217–233.
- EICHENSEER, H.T.H., WALGENWITZ, F.R., AND BONDI, P.J., 1999, Stratigraphic control on facies and diagenesis of dolomitized oolitic siliciclastic ramp sequences (Pinda Group, Albian, Offshore Angola): *American Association of Petroleum Geologists, Bulletin*, v. 83, p. 1729–1758.
- FEDORCHUK, N.D., 2014, Evaluating the biogenicity of fluvial–lacustrine stromatolites from the Mesoproterozoic Copper Harbor Conglomerate, Upper Peninsula of Michigan [MSc Thesis]: University of Wisconsin, Milwaukee, 59 p.
- FOUKE, B.W., 2011, Hot-spring systems geobiology: abiotic and biotic influences on travertine formation at Mammoth Hot Springs, Yellowstone National Park, USA: *Sedimentology*, v. 58, p. 170–219.
- FROGLEY, M.R., GRIFFITHS, H.I., AND MARTENS, K., 2002, Modern and fossil ostracodes from ancient lakes, in Holmes, J.A., and Chivas, A.R., eds., *The Ostracoda: Applications in Quaternary Research*: American Geophysical Union, *Geophysical Monograph Series* 131, p. 167–184.
- FURQUIM, S.A.C., GRAHAM, R.C., BARBIERI, L., DE QUEIROZ NETO, J.P., AND VALLÉS, V., 2008, Mineralogy and genesis of smectites in an alkaline–saline environment of Pantanal wetland, Brazil: *Clays and Clay Minerals*, v. 56, p. 579–595.
- GARCIA-RUIZ, J.M., 2000, Geochemical scenarios for the precipitation of biomimetic inorganic carbonates, in Grotzinger, J.P., and James, N.P., eds., *Carbonate Sedimentation and Diagenesis in the Evolving Precambrian World*: Society for Sedimentary Geology, Special Publication 67, p. 75–89.
- GIERLowski-KORDESCH, E.H., 2009, Lacustrine Carbonates, in Alonso-Zarza, A.M., and Tanner, L.H., eds., *Carbonates in Continental Settings*: Amsterdam, Elsevier, *Developments in Sedimentology* 61, p. 1–101.
- GOLDBERG, K., KUCHLE, J., SCHERER, C., ALVARENGA, R., ENE, P.L., ARMELENTI, G., AND DE ROS, L.F., 2017, Re-sedimented deposits in the rift section of the Campos Basin: *Marine and Petroleum Geology*, v. 80, p. 412–431.
- GROTZINGER, J.P., AND KNOLL, A.H., 1995, Anomalous carbonate precipitates: Is the Precambrian the key to the Permian? *Palaio*, v. 10, p. 578–96.
- GROTZINGER, J.P., AND KNOLL, A.H., 1999, Stromatolites in Precambrian carbonates: evolutionary mileposts or environmental dipsticks? *Annual Review of Earth and Planetary Sciences*, v. 27, p. 313–358.
- GUARDADO, L.R., SPADINI, A.R., BRANDÃO, J.S.L., AND MELO, M.R., 2000, Petroleum system of the Campos Basin, in Mello, M.R., and Katz, B., eds., *Petroleum System of South Atlantic Margins*: American Association of Petroleum Geologists, *Memoir* 73, p. 317–324.
- HARRIS, N., SORRIAUX, P., AND TOOMEY, D.F., 1994, Geology of the Lower Cretaceous Viodo carbonate, Congo basin: a lacustrine carbonate in the South Atlantic rift, in Lamontado, A.J., Schreiber, B., and Harris, P.M., eds., *Lacustrine Reservoirs and Depositional Systems*: Society for Sedimentary Geology, *Core Workshop* 19, p. 143–172.
- HASSALL, J., FERRARIS, P., AL-RAISI, M., HURLEY, N.F., BOYD, A., AND ALLEN, D.F., 2004, Comparison of permeability predictors from NMR, formation image and other logs in a carbonate reservoir: Abu Dhabi, Society of Petroleum Engineers, *International Conference and Exhibition*, p. 1–12.
- HESSE, R., 1989, Silica diagenesis: origin of inorganic and replacement cherts: *Earth-Science Reviews*, v. 26, p. 253–284.
- HEWARD, A.P., CHUENBUNCHOM, S., MAKEL, G., MARSLAND, D., AND SPRING, L., 2000, Nang Nuan oil field, B6/27, Gulf of Thailand: karst reservoirs of meteoric or deep-burial origin? *Petroleum Geoscience*, v. 6, p. 15–27.
- JAMES, N., AND CHOQUETTE, P.W., 1984, Diagenesis 9, Limestones: The Meteoric Diagenetic Environmental: *Geoscience Canada*, v. 11, p. 161–194.
- JONES, B.F., 1986, Clay mineral diagenesis in lacustrine sediments, in Mumpton, F.A., ed., *Studies in Diagenesis*, v. 1578: U.S. Geological Survey, *Bulletin*, p. 291–300.
- JONES, B., AND RENAUT, R.W., 1994, Crystal fabrics and microbiota in large pisoliths from Laguna Pastos Grandes, Bolivia: *Sedimentology*, v. 41, p. 1171–1202.
- KARNER, G., AND DRISCOLL, N., 1999, Tectonic and stratigraphic development of the West African and eastern Brazilian margins: insights from quantitative basin modelling, in Cameron, N., Bate, R., and Clure, V., eds., *The Oil and Gas Habitats of the South Atlantic*: Geological Society of London, *Special Publication* 153, p. 11–40.
- KARNER, G.D., AND GAMBÓA, L.A.P., 2007, Timing and origin of the South Atlantic pre-salt sag basins and their capping evaporites, in Schreiber, B.C., Lugli, S., and Babel, M., eds., *Tectonics, Basin Evolution and Evaporites*: Geological Society of London, *Special Publication* 285, p. 15–35.
- KENDALL, A., 1977, Fasicular-optic calcite: a replacement of bundled acicular carbonate cements: *Journal of Sedimentary Petrology*, v. 47, p. 1056–1062.
- KHALAF, F.I., 1988, Petrography and diagenesis of silcrete from Kuwait, Arabian Gulf: *Journal of Sedimentary Petrology*, v. 58, p. 1014–1022.
- LÖNOY, A., 2006, Making sense of carbonate pore systems: *American Association of Petroleum Geologists, Bulletin*, v. 90, p. 1381–1405.
- LUCIA, F.J., 1995, Rock-fabric/petrophysical classification of carbonate pore space for reservoir characterization: *American Association of Petroleum Geologists, Bulletin*, v. 79, p. 1275–1300.
- MACHEL, H.G., 2005, Investigations of burial diagenesis in carbonate hydrocarbon reservoir rocks: *Geoscience Canada*, v. 32, p. 103–128.
- MACHEL, H.G., AND LÖNNIE, J., 2002, Hydrothermal dolomite: a product of poor definition and imagination: *Sedimentary Geology*, v. 152, p. 163–171.
- MAZZULLO, S.J., 2004, Overview of porosity evolution in carbonate reservoirs: *Kansas Geological Society, Bulletin* 79, 19 p.
- MAZZULLO, S.J., AND HARRIS, P.M., 1991, An overview of dissolution porosity development in the deep-burial environment, with examples from carbonate reservoirs in the Permian Basin, in Candelaria, M., ed., *Permian Basin Plays: Tomorrow's Technology Today*: West Texas Geological Society, p. 125–138.
- MCKENZIE, D., 1978, Some remarks on the development of sedimentary basins: *Earth and Planetary Science Letters*, v. 40, p. 25–32.
- MCKENZIE, J., AND VASCONCELOS, C., 2009, Dolomite Mountains and the origin of the dolomite rock of which they mainly consist: historical developments and new perspectives: *Sedimentology*, v. 56, p. 205–219.
- MEISLING, K.E., COBBOLD, P.R., AND MOUNT, V.S., 2001, Segmentation of an obliquely rifted margin, Campos and Santos basins, southeastern Brazil: *American Association of Petroleum Geologists, Bulletin*, v. 85, p. 1925–1944.
- MEISTER, P., JOHNSON, O., CORSETTI, F., AND NEALSON, K.H., 2011, Magnesium inhibition controls spherical carbonate precipitation in ultrabasic springwater (Cedars, California) and culture experiments, in Reitner, J., Quéric, N.V., and Arp, G., eds., *Advances in Stromatolite Geobiology*: Berlin, Springer, *Lecture Notes in Earth Sciences* 131, p. 101–121.
- MIZUSAKI, A.M.P., THOMAZ FILHO, A., AND VALENÇA, J., 1988, Volcano-sedimentary sequence of Neocomian age in Campos Basin (Brazil): *Revista Brasileira de Geociências*, v. 18, p. 247–251.
- MOHRIAK, W., NEMCOK, M., AND ENCISO, G., 2008, South Atlantic divergent margin evolution: rift-border uplift and salt tectonics in the basins of SE Brazil, in Pankhurst, R.J., Trouw, R.A.J., Brito Neves, B.B., and De Wit, M.J., eds., *West Gondwana: Pre-Cenozoic Correlations Across the South Atlantic Region*: Geological Society of London, *Special Publication* 294, p. 365–398.
- MOORE, C.H., 2001, Carbonate Reservoirs: Porosity Evolution and Diagenesis in a Sequence Stratigraphic Framework: Amsterdam, Elsevier, *Developments in Sedimentology* 67, 444 p.
- MOORE, C.H., AND WADE, W.J., 2013, Carbonate Reservoirs: Porosity and Diagenesis in a Sequence Stratigraphic Framework: Amsterdam, Elsevier, *Developments in Sedimentology* 55, 392 p.
- MORSE, J.W., AND MACKENZIE, F., 1990, Geochemistry of Sedimentary Carbonates: Amsterdam, Elsevier, 706 p.
- MOUNTJOY, E.W., AND MARQUEZ, X.M., 1997, Predicting reservoir properties in dolomites: Upper Devonian Leduc Buildups, Deep Alberta Basin, in Kupecz, J., Guyas, J., and Block, S., eds., *Reservoir Quality Prediction in Sandstones and Carbonates*: American Association of Petroleum Geologists, *Memoir* 69, p. 267–306.
- MOURA, J., AND PRAÇA, U., 1985, Ostracodes das seqüências não marinhas e transicionais Mesozóicas (Andares Jiquiá e Alagoas), Bacia de Campos, in Coletânea de Trabalhos Paleontológicos: Departamento Nacional da Produção Mineral, Ministério das Minas e Energia, Brasília, Série Geologia 27, p. 401–408.
- MUNIZ, M.C., 2014, Tectono-stratigraphic evolution of the Barremian–Aptian Continental Rift Carbonates in Southern Campos Basin, Brazil [PhD Thesis]: Royal Holloway University of London, 324 p.
- MUNIZ, M.C., AND BOSENCE, D.W.J., 2015, Pre-salt microbialites from the Campos Basin (offshore Brazil): image log facies, facies model and cyclicity in lacustrine carbonates, in Bosence, D.W.J., Gibbons, K.A., Le Heron, D.P., Morgan, W.A., Pritchard, T., and Vining, B.A., eds., *Microbial Carbonates in Space and Time: Implications for Global Exploration and Production*: Geological Society of London, *Special Publication* 418, p. 221–242.
- MURRAY, R.C., 1990, Diagenetic silica stratification in a paleosilcrete, North Texas: *Journal of Sedimentary Petrology*, v. 60, p. 717–720.

- NÜRNBERG, D., AND MÜLLER, R.D., 1991, The tectonic evolution of the South Atlantic from Late Jurassic to present: *Tectonophysics*, v. 191, p. 27–53.
- ODIN, G.S., 1988, Green Marine Clays: Amsterdam, Elsevier, Developments in Sedimentology 45, 444 p.
- PLATT, N.H., AND WRIGHT, V.P., 1991, Lacustrine carbonates: facies models, facies distributions and hydrocarbon aspects, in Anadón, P., Cabrera, L., and Kelts, K., eds., *Lacustrine Facies Analysis*: International Association of Sedimentologists, p. 57–74.
- POPE, M.C., GROZINGER, J.P., AND SCHREIBER, B.C., 2000, Evaporitic subtidal stromatolites produced by in situ precipitation: textures, facies associations, and temporal significance: *Journal of Sedimentary Research*, v. 70, p. 1139–1151.
- POZO, M., AND CASAS, J., 1999, Origin of kerolite and associated Mg clays in palustrine-lacustrine environments. The Esquivias deposit (Neogene Madrid Basin, Spain): *Clay Minerals*, v. 34, p. 395–418.
- RABINOWITZ, P.D., AND LABRECQUE, J., 1979, The Mesozoic South Atlantic Ocean and evolution of its continental margins: *Journal of Geophysical Research*, v. 84, p. 5973–6002.
- RACEY, A., BAILEY, H.W., BECKETT, D., GALLAGHER, L.T., HAMPTON, M.J., AND MCQUILKEN, J., 2001, The petroleum geology of the Early Eocene El Garia Formation, Hasdrubal Field, Offshore Tunisia: *Journal of Petroleum Geology*, v. 24, p. 29–53.
- REHIM, H., MIZUSAKI, A.M.P., CARVALHO, M.D., AND MONTEIRO, M., 1986, Talco e estevensita na Formação Lagoa Feia da Bacia de Campos: possíveis implicações no ambiente deposicional: XXXIV Congresso Brasileiro de Geologia: p. 416–424.
- RENAUT, R.W., TIERCELIN, J.J., AND OWEN, R.B., 1986, Mineral precipitation and diagenesis in the sediments of the Lake Bogoria basin, Kenya Rift Valley, in Frostick, L., ed., *Sedimentation in the African Rift*: Geological Society of London, Special Publication 25, p. 159–175.
- REZENDE, M.F., AND POPE, M.C., 2015, Importance of depositional texture in pore characterization of subsalt microbialite carbonates, offshore Brazil, in Bosence, D.W.J., Gibbons, K.A., Le Heron, D.P., Morgan, W.A., Pritchard, T., and Vining, B.A., eds., *Microbial Carbonates in Space and Time: Implications for Global Exploration and Production*: Geological Society of London, Special Publication 418, p. 193–207.
- RIDING, R., 2000, Microbial carbonates: the geological record of calcified bacterial-algal mats and biofilms: *Sedimentology*, v. 47, p. 179–214.
- RIDING, R., 2008, Abiogenic, microbial and hybrid authigenic carbonate crusts: components of Precambrian stromatolites: *Geologia Croatica*, v. 61, p. 73–103.
- RIDING, R., AND LIANG, L., 2005, Geobiology of microbial carbonates: metazoan and seawater saturation state influences on secular trends during the Phanerozoic: *Palaeogeography, Palaeoclimatology, Palaeoecology*, v. 219, p. 101–115.
- ROBERTS, J.A., KENWARD, P.A., FOWLE, D.A., GOLDSTEIN, R.H., GONZALEZ, L.A., AND MOORE, D.S., 2013, Surface chemistry allows for abiotic precipitation of dolomite at low temperature: *National Academy of Sciences [USA], Proceedings*, v. 110, p. 14540–14545.
- ROSENDAHL, B., MOHRIAK, W., NEMCOK, M., ODEGARD, M., TURNER, J., AND DICKSON, W., 2005, West African and Brazilian conjugate margins: crustal types, architecture, and plate configurations: 4th HGS/PESGB International Conference on African Exploration and Production.
- ROSS, G., AND CHIARENZELLI, J., 1985, Paleoclimatic significance of widespread Proterozoic silcretes in the Bear and Churchill Provinces of the Northwestern Canadian Shield: *Journal of Sedimentary Petrology*, v. 55, p. 196–204.
- SALLET, A., RUSHTON, S., BUAMBUA, L., INMAN, K., MCNEIL, R., AND DICKSON, J.A.D., 2016, Presalt stratigraphy and depositional systems in the Kwanza Basin, offshore Angola: *American Association of Petroleum Geologists, Bulletin*, v. 100, p. 1135–1164.
- SCHALLER, H., 1973, Estratigrafia da Bacia de Campos: XXVII Congresso Brasileiro de Geologia, Proceedings, p. 247–258.
- SHTUKENBERG, A.G., PUNIN, Y.O., GUNN, E., AND KAHR, B., 2012, Spherulites: *Chemical Reviews*, v. 112, p. 1805–1838.
- SILVA-TELLES, A.C., 1992, Novo zoneamento de sequência das coquinas da Formação Lagoa Feia (Neojiquia da Bacia de Campos) com base em ostracodes: aspectos evolutivos: São Paulo, 37º Congresso Brasileiro de Geologia, Proceedings, p. 489–490.
- SPADAFORA, A., PERRI, E., MCKENZIE, J.A., AND VASCONCELOS, C., 2010, Microbial biomineralization processes forming modern Ca:Mg carbonate stromatolites: *Sedimentology*, v. 57, p. 27–40.
- SPÖL, C., AND PITMAN, J.K., 1998, Saddle (baroque) dolomite in carbonates and sandstones: a reappraisal of the burial-diagenetic concept, in Morad, S., ed., *Carbonate Cementation in Sandstones: International Association of Sedimentologists, Special Publication 26*, p. 437–460.
- SZATMARI, P., 2000, Habitat of petroleum along the South Atlantic margins, in Mello, M., and Katz, B., eds., *Petroleum Systems of South Atlantic Margins: American Association of Petroleum Geologists, Memoir 73*, p. 69–75.
- TORSVIK, T.H., ROUSSE, S., LABAILS, C., AND SMETHURST, M.A., 2009, A new scheme for the opening of the South Atlantic Ocean and the dissection of an Aptian salt basin: *Geophysical Journal International*, v. 177, p. 1315–1333.
- TOSCA, N.J., AND MASTERTON, A.L., 2014, Chemical controls on incipient Mg-silicate crystallization at 25°C: implications for early and late diagenesis: *Clay Minerals*, v. 49, p. 165–194.
- TOSCA, N.J., AND WRIGHT, V.P., 2014, The formation and diagenesis of Mg-clay minerals in lacustrine carbonate reservoirs: *American Association of Petroleum Geologists, Annual Convention and Exhibition*.
- TOSCA, N.J., AND WRIGHT, V.P., 2015, Diagenetic pathways linked to labile Mg-clays in lacustrine carbonate reservoirs: a model for the origin of secondary porosity in the Cretaceous pre-salt Barra Velha Formation, offshore Brazil, in Armitage, P.J., Butcher, A.R., Churchill, J.M., Csoma, A.E., Hollis, C., Lander, R.H., Omma, J.E., and Worden, R.H., *Reservoir Quality of Clastic and Carbonate Rocks: Analysis, Modelling and Prediction*: Geological Society of London, Special Publication 435, doi.org/10.1144/SP435.1.
- TUCKER, M.E., AND WRIGHT, V.P., 1991, *Carbonate Sedimentology*: Oxford, UK, Blackwell Scientific Publications, 482 p.
- TURNER, S., REGELOUS, M., KELLEY, S., HAWKESWORTH, C., AND MANTOVANI, M., 1994, Magmatism and continental break-up in the South Atlantic: high precision ^{40}Ar – ^{39}Ar geochronology: *Earth and Planetary Science Letters*, v. 121, p. 333–348.
- VAN DER LAND, C., WOOD, R., WU, K., VAN DUKE, M.J., JIANG, Z., CORBETT, P.W.M., AND COUPLES, G., 2013, Modelling the permeability evolution of carbonate rocks: *Marine and Petroleum Geology*, v. 48, p. 1–7.
- VAN HOUTEN, F.B., AND PURUCKER, M.E., 1984, Glauconite peloids and chamosite ooids: favourable factors, constraints and problems, *Earth-Science Reviews*, v. 20, p. 211–243.
- VASCONCELOS, C., WARTHMANN, R., MCKENZIE, J.A., VISSCHER, P.T., BITTERMANN, A.G., AND VAN LITH, Y., 2006, Lithifying microbial mats in Lagoa Vermelha, Brazil: Modern Precambrian relics? *Sedimentary Geology*, v. 185, p. 175–183.
- VINCENS, A., CASANOVA, J., AND TIERCELIN, J.J., 1986, Palaeolimnology of lake bogoria (Kenya) during the 4500 BP High lacustrine phase, in Frostick, L., ed., *Sedimentation in the African Rifts: Geological Society of London, Special Publication 25*, p. 323–330.
- WARREN, J.K., 2006, *Evaporites: Sediments, Resources and Hydrocarbons*: Berlin, Springer Science, 1035 p.
- WEGER, R.J., EBERLI, G.P., BAECHLE, G.T., MASSAFERRO, J.L., AND SUN, Y., 2009, Quantification of pore structure and its effect on sonic velocity and permeability in carbonates: *American Association of Petroleum Geologists, Bulletin*, v. 93, p. 1297–1317.
- WHITE, N., AND MCKENZIE, D., 1988, Formation of the “steer’s head” geometry of sedimentary basins by differential stretching of the crust and mantle: *Geology*, v. 16, p. 250–253.
- WINTER, W.R., JAHNERT, R.J., AND FRANÇA, A.B., 2007, Bacia de Campos: *Boletim de Geociências da Petrobras*, v. 15, p. 511–529.
- WRIGHT, V.P., 2011, Reservoir architectures in non-marine carbonates: *American Association of Petroleum Geologists, Annual Convention and Exhibition, Proceedings*, p. 75–89.
- WRIGHT, V.P., 2012, Lacustrine carbonates in rift settings: the interaction of volcanic and microbial processes on carbonate deposition, in Garland, J., Neilson, J.E., Laubach, S., and Whidden, K.J., eds., *Advances in Carbonate Exploration and Reservoir Analysis: Geological Society of London, Special Publication 370*, p. 39–47.
- WRIGHT, V.P., 2013, To be or not to be, microbial: Does it matter?: *Microbial Carbonates in Space and Time Conference, Geological Society of London, Abstracts volume*.
- WRIGHT, V.P., AND BARRETT, A.J., 2015, An abiotic model for the development of textures in some South Atlantic Early Cretaceous lacustrine carbonates, in Grotzinger, J.P., and James, N., eds., *Microbial Carbonates in Space and Time: Implications for Global Exploration and Production: The Geological Society of London, Special Publication 418*, p. 209–219.

Received 4 July 2016; accepted 10 October 2017.